FFNo 672 Aug 65

NF01131

DEPARTMENT OF MECHANICAL ENGINEERING AND MECHANICS
SCHOOL OF ENGINEERING
OLD DOMINION UNIVERSITY
NORFOLK, VIRGINIA

COMPARATIVE STUDY OF FLARE CONTROL LAWS

By

A.A. Nadkarni, Principal Investigator

Final Report
For the period December 15, 1979 - October 15, 1981

Prepared for the
National Aeronautics and Space Administration
Langley Research Center
Hampton, Virginia

October 1981

DEPARTMENT OF MECHANICAL ENGINEERING AND MECHANICS
SCHOOL OF ENGINEERING
OLD DOMINION UNIVERSITY
NORFOLK, VIRGINIA

COMPARATIVE STUDY OF FLARE CONTROL LAWS

By

A.A. Nadkarni, Principal Investigator

Final Report
For the period December 15, 1979 - October 15, 1981

Prepared for the
National Aeronautics and Space Administration
Langley Research Center
Hampton, Virginia

Under
Research Grant NSG 1480
J.F. Creedon, Technical Monitor
Flight Electronics Division

Submitted by the
Old Dominion University Research Foundation
P.O. Box 6369
Norfolk, Virginia 23508-0369

October 1981

TABLE OF CONTENTS

LIST OF TABLES

LIST OF FIGURES

LIST OF FIGURES (CONTINUED)

LIST OF FIGURES (CONCLUDED)

COMPARATIVE STUDY OF FLARE CONTROL LAWS

By

Arun A. Nadkarni*

INTRODUCTION

This report presents the development of a digital, 3-D, automatic
control law designed to achieve an optimal transition of a B-737 aircraft
between glide slope conditions and the desired final touchdown condition.
The digital control law developed here is a time-invariant, state-estimate
feedback law, and the design is capable of using the Microwave Landing
System (MLS) under development by the Federal Aviation Agency (FAA). The
study of a curved flight path leading to a steep final approach and touch-
down under low visibility conditions is part of the Terminal Configured
Vehicle (TCV) program, sponsored by NASA/Langley Research Center (LaRC).
The goals of this program include the reduction of aircraft noise in
communities surroundings airports, the reduction of fuel consumption, the
reduction of the effects of adverse weather conditions on aircraft opera-
tions, and the efficient use of airspace in congested terminal areas. A
specific objective which supports these goals is the development of the
capability to perform automatic flares from steep glide slopes to precise
touchdown locations.

The major reason for the use of steep glide slopes is the resultant
noise reduction in comparison with the currently used 2.5° to 3° glide
slopes with the Instrument Landing System (ILS). The steeper glide slope
reduces the noise levels perceived on an identical segment of the ground
for two reasons: first, at equal distances from the touchdown point, the
aircraft flying a steeper, say a six-degree glide slope, is at about twice
the altitude compared to that flying a three-degree glide slope. This
difference in altitude causes a considerable reduction in the noise
level perceived on the ground even if the two sources generate identical

*Visiting Assistant Professor, Department of Mechanical Engineering and
 Mechanics, Old Dominion University, Norfolk, Virginia 23508.

noise levels. Second, an aircraft flying a steeper glide slope requires a
lower thrust setting, and this causes further reduction in the noise level
perceived on the ground. The reduction in thrust setting has the added
advantages of reducing the fuel consumption during the final phase of the
flight path. The ability to fly varying glide slopes may also provide an
effective method to avoid encountering vortices generated by larger
aircraft. This versatility may result in a more efficient use of the
airspace.

This is not without its attendent disadvantages. The use of steeper
glide slopes for noise reduction requires that the aircraft be flown in a
high-drag, low-power-setting configuration. In addition to this situation,
the higher sink rates associated with these paths allow pilots considerably
less reaction time to recognize an emergency and to take appropriate
corrective actions in the event of atmospheric disturbances (e.g., gusts,
wind shears, etc.), system or sensor failures, etc.

There is also a need for reducing touchdown dispersions in the
presence of varying flight conditions encountered during the flare portion
of the landing. The reduction in the touchdown dispersions greatly
facilitates high-speed rollout, which significantly increases the traffic-
handling capacity of the terminal. It is obvious that developing
capability to perform automatic flare maneuvers will accomplish many of
these goals.

In the next section, "Description of the System Model," the system
equations of motion of the aircraft are presented. These linear equations
represent the perturbed motion of the aircraft from the nominal glide slope
trajectory. A method of incorporating the spatial, low-level wind shears
into these perturbed equations of motion is indicated. It is shown that
the system equations then assume the familiar form of the linear regulator
problem, acted upon by a constant disturbance. Under "Derivation of the
Control Law," a design procedure to compute a digital, time-invariant,
optimal control law for the discrete regulator problem acted upon by a
constant disturbance is indicated. This is followed by a section
describing implementation of the control law. Under "Results," performance
curves are presented to show the capability of this digital, state-feedback

2

controller to perform the optimal flare maneuvers in the presence of various wind shear conditions indicated. In the final section the conclusions derived from the study of the automated flare maneuvers are listed along with scope for further work.

DESCRIPTION OF THE SYSTEM MODEL

Introduction

The development of the mathematical model in this study follows closely the development of a similar model described in detail in references 1 to 6. The complete derivation of the system equations is described in these references; however, a brief outline of the derivation is given below for the sake of completeness.

Aircraft Dynamics with Wind Disturbances

This study is concerned only with the final phase of flight, viz the flare. Thus, the aircraft is approaching the runway on a certain initial glidepath. The aircraft is aligned with the runway, has a zero or at most a very small yaw angle with respect to the runway as well as a zero bank (or roll) angle, except in the case of a significant crosswind. Therefore, all the lateral dynamics are neglected during the analysis and only longitudinal dynamics are considered.

With these assumptions and assuming small perturbations about the nominal path, the nonlinear equations of motion of the aircraft can be linearized using well-known methods. The complete equations of motion and the linearization procedure are outlined in references 5 to 7. These nonlinear equations are derived assuming (1) a flat earth, (2) an earth-fixed frame of reference, (3) a rigid aircraft, and (4) that second-order terms are neglected. These equations of motion are coupled. However, for a steady-state flight condition, the equations can be decoupled into two groups, the longitudinal equations and the lateral equations of motion. As already indicated, only longitudinal equations of motion are dealt with in this study.

3

The decoupled, nonlinear longitudinal equations of motion are then linearized about the nominal trajectory (i.e., the steady-state flight of $-3°$, $-6°$ glide slope, etc.) to obtain the linear perturbation equations in the state variable form. The equations are expressed in a stability axes coordinate frame attached to the aircraft at the center of mass (fig. 1).

The final linearized, longitudinal equations of motion, including wind disturbances, assume the following standard form (refs. 1-4):

$$\dot{x} = Ax + Bu + Dw \tag{1a}$$

where

$$x = (\theta \; u' \; \alpha \; q \; \frac{x - x_0}{U_0} \; \frac{z - z_0}{U_0} \; \delta T \; \delta th \; \delta s \; \delta e)^T \tag{1b}$$

$$u = (\dot{\delta e} \; \dot{\delta s} \; \delta th \; \delta_{sp})^T \tag{1c}$$

and

$$w = (u_w' \; \alpha_w \; q_w)^T \tag{1d}$$

where the states (x's) and the controls (u's) are

θ = perturbation in pitch angle

u' = perturbation in velocity along x_s (stability) axis normalized

α = perturbation in angle of attack

q = perturbation in the pitch rate

$\frac{x - x_0}{U_0}$ = perturbation in the horizontal position of the aircraft (normalized), in inertial frame

$\frac{z - z_0}{U_0}$ = perturbation in the vertical position of the aircraft (normalized), in inertial frame

δT = perturbation in the thrust

δth = perturbation in the throttle position

δs = perturbation in stabilizer position

4

δe = perturbation in the elevator position

$\dot{\delta e}$ = perturbation in the elevator rate

$\dot{\delta s}$ = perturbation in the stabilizer rate

$\dot{\delta th}$ = perturbation in the throttle rate

δsp = perturbation in spoiler position

The subscript w indicates the perturbation in the variable due to wind disturbances. Note that, out of the 10 variables in the state vector x, the first 4 variables are sufficient to describe the longitudinal perturbed motion of the aircraft. The next two variables   viz $\dfrac{x - x_o}{U_o}$ and $\dfrac{z - z_o}{U_o}$ are defined for designing a 4-D control law to minimize the deviations from the nominal path, if desired. The perturbation in the thrust is defined as a state variable in order to model the thrust dynamics taking the "spool up" time of the engine into account, at least linearly. The last three variables, the perturbations in the position of the throttle, the stabilizer, and the elevator, were added as a result of the design decision to command the rates of these controls.

The position of the spoiler was included as a control variable in case it is decided to study the effects of direct lift control in future studies. In the present work, however, the spoiler was made inoperative during the simulation runs.

Wind Model

In order to complete and simulate the system model given by equation (1), the wind perturbation vector w must be specified. The components of this vector consist of u'_w, the normalized wind velocity in the $+x_s$ direction; α_w, the perturbation in the angle of attack due to the wind; and q_w, the perturbation in the pitch rate of the aircraft due to wind. These wind variables may be logically modeled as the sum of a gust component with zero mean value and a steady component.

The gust components are modeled using the well-known Dryden spectrum (refs. 5-7). This method consists of using spectral factorization methods to obtain a dynamical system which generates a random process having the specified power spectral density when driven by white noise. Because of

the linearity of the system, the three gust components can be treated individually; thus, only appropriate components are included in the longitudinal equations (eqs. (1a) - (1d)). The detailed derivation of the gust components can be found in references 3 to 6 and will not be given here.

The Dryden spectra describe the statistical behavior of the wind gust velocities in the aircraft body-fixed coordinates, and the gust components can be expressed in the following form (refs. 3-7):

$$\dot{W}_g = A_{ww} W_g + B_{\xi 1} \xi_1 \tag{2}$$

where

$$W_g = (\alpha_{gb} \ \dot{\alpha}_{gb} \ q_{gb} \ u_{gb})^T$$

These four gust components constitute the four components (x_{11} to x_{14}) of the state vector. The elements of A_{ww} and $B_{\xi 1}$ can be obtained from reference 3.

The steady-state components of the wind are simpler to model since they do not involve spectral factorization. These components can be modeled as the output of a first order deterministic plant, corrupted by a white noise. This can be done in different ways (refs. 3 and 4).

To permit modeling of spatial shears, a new method was proposed (refs. 8-10). The model also makes the whole system controllable, and the feedback gain matrix can be computed as is done in the usual manner for the regulator problems without the need for splitting the matrix Riccati equation in two.

Let the aircraft be coming down on a nominal glide slope in a steady flight condition. Also, for simplicity, let the aircraft be flying in a disturbance-free atmosphere $\{t = s, s < 0\}$. (It is noted that the method can be trivially extended to the situation when the aircraft is flying in a constant wind, for $\{t = s, s < 0\}$.) Now, at $t = 0$ let the aircraft encounter a step wind, with a component U_{w_o} in the $+x_e$ direction and a component W_{w_o} in the $+z_e$ direction. Also, let the subsequent wind field be

6

described by a linear shear profile with a shear rate of X kn/30.48 m (100 ft) in the horizontal wind velocity, and Z kn/30.48 m (100 ft) in the vertical wind velocity. In the present notation, $U_{w_o} > 0$ represents a tailwind, $W_{w_o} > 0$ represents a downdraft, $X > 0$ represents a linear increase in tailwind (with decreasing height), and $Z > 0$ represents a linear increase in downdraft (with decreasing height) as seen by an earth-fixed observer. Then the rate of change of the perturbation wind velocity in the horizontal direction (after normalizing with $U_{i_o}^s$) is given by (ref. 10):

$$\dot{u}_w' = - \frac{X}{100} \ (\cos \gamma_o \cdot \theta + \sin \gamma_o \cdot u' - \cos \gamma_o \cdot \alpha) \tag{3}$$

Similarly, the rate of change of the normalized perturbation wind velocity in the vertical direction is given by

$$\dot{w}_w' = - \frac{Z}{100} \ (\cos \gamma_o \cdot \theta + \sin \gamma_o \cdot u' - \cos \gamma_o \cdot \alpha) \tag{4}$$

Note that equations (3) and (4) yield the perturbation components of the wind at the wing. However, due to inertia effects, the flow field over the wing does not sense these changes until it travels a few chord lengths (ref. 5). These inertia effects can be modeled by a first-order lag term with an appropriate time constant. Thus, the steady-state components of the perturbation wind velocity in a shear field can be modeled as

$$\dot{x}_{15} = a_1 x_{15} + b_1 x_{17}$$

$$\dot{x}_{16} = a_1 x_{16} + b_1 x_{18}$$

$$\dot{x}_{17} = - \frac{X}{100} \ (\cos \gamma_o \cdot \theta + \sin \gamma_o \cdot u' - \cos \gamma_o \cdot \alpha)$$

$$\dot{x}_{18} = - \frac{Z}{100} \ (\cos \gamma_o \cdot \theta + \sin \gamma_o \cdot u' - \cos \gamma_o \cdot \alpha) \tag{5}$$

where

7

x_{15} = horizontal component of actual perturbation wind velocity felt by the wing, u'_{w_a}

x_{16} = vertical component of actual perturbation wind velocity felt by the wing, w'_{w_a}

x_{17} = horizontal component of perturbation wind velocity at the wing, $u'_{w'}$, and

x_{18} = vertical component of perturbation wind velocity at the wing, w'_{w}

The 4 steady-state variables can now be augmented with the 10 aircraft states (eqs. (1a) - (1d)) and 4 gust components to yield the complete state variable model of the aircraft motion in the presence of atmospheric disturbance.

The system model developed above is completely controllable in addition to being more realistic than the previous attempts to model the atmospheric disturbance effects. The optimal, constant feedback gain matrix for this system can now be computed in the usual way as for a regulator problem, with the two nominal shear components acting as constant disturbances on the system. The method to compute the gain matrix is described in detail under "Derivation of the Control Law."

The Basic Augmented System: Aircraft in a Wind Disturbance Field

With the derivation of the wind model for steady wind velocity components now complete, it is possible to augment the wind model (eq. (5)) with the aircraft equations of motion in presence of wind disturbances (eqs. (1a) - (1d)) to yield the state equations of the basic augmented system.

The final form of the wind model assumes the following form:

$$\dot{W}_g = A_{ww} W_g + B_{\xi 1} \xi_1 \tag{6}$$

$$\dot{W}_s = A_{wx} x + B_{\xi 2} \xi_2 + B_w W_d \tag{7}$$

where ξ's are white noise processes to account for the unknown disturbances and the wind vectors are

$$W_g = (\alpha_{gb} \quad \dot{\alpha}_{gb} \quad q_{gb} \quad u'_{gb})^T$$

$$W_s = (u'_w \quad w'_w \quad u'_{w_a} \quad w'_{w_a})^T$$

Here the subscripts g and s refer to gust and steady components, respectively. The elements of the matrices A_{ww}, $B_{\xi 1}$, and $B_{\xi 2}$ can be obtained from references 3 and 4. The elements of the A_{wx} and B_w can be obtained from equation (5) and references 9 and 10.

Defining a composite wind vector

$$W \triangleq (W_g^T \quad W_s^T)^T \tag{8}$$

the wind vector w defined in equation (1) can be expressed as

$$w = \begin{bmatrix} C_{wg} & C_{ws} \end{bmatrix} \begin{Bmatrix} W_g \\ W_s \end{Bmatrix} \tag{9}$$

where $\begin{bmatrix} C_{wg} & C_{ws} \end{bmatrix}$ is an appropriate transformation matrix (ref. 3). The steady winds, the wind shears, and the gusts can now be included in the system equations (1a) to (1d).

The complete system equations, with the inclusion of the wind model, can now be expressed in the standard state variable form as

$$\begin{Bmatrix} \dot{x} \\ \dot{W}_g \\ \dot{W}_s \end{Bmatrix} = \begin{bmatrix} A & DC_{wg} & DC_{ws} \\ 0 & A_{ww} & 0 \\ A_{wx} & 0 & 0 \end{bmatrix} \begin{Bmatrix} x \\ W_g \\ W_s \end{Bmatrix} + \begin{bmatrix} B \\ 0 \\ 0 \end{bmatrix} u + \begin{bmatrix} 0 \\ 0 \\ B_w \end{bmatrix} W_d + \begin{bmatrix} 0 & 0 \\ B_{\xi 1} & 0 \\ 0 & B_{\xi 2} \end{bmatrix} \begin{Bmatrix} \xi_1 \\ \xi_2 \end{Bmatrix}$$

or

$$\dot{\bar{x}} = \bar{A}\,\bar{x} + \bar{B}\,u + \bar{B}_w\,W_d + \bar{B}_\xi\,\xi \qquad (10)$$

DERIVATION OF THE CONTROL LAW

It is now possible to undertake the design of the optimal control law for the above problem by invoking the separation theorem in the usual manner. The general approach to study the flare performance (refs. 1, 2, 8) is briefly as follows. The longitudinal equations of motion of the aircraft (eq. (10)), which are perturbations about the nominal glide slope trajectory, are discretized (ref. 11). The constant gain, state feedback optimal control law, designed in a manner described below, is incorporated into the system equations, and the system is expressed as a deterministic closed-loop system. The difference between the initial glide slope and the desired touchdown conditions is supplied as initial condition x_o, and the time response of the deterministic closed-loop system is simulated on a digital computer (refs. 8, 9, 12).

The complete system equations for the augmented system can be expressed in discretized form as (refs. 8-10):

$$\begin{Bmatrix} x_{k+1} \\ u_{1_{k+1}} \end{Bmatrix} = \begin{bmatrix} F & G \\ F_{11} & F_{12} \end{bmatrix} \begin{Bmatrix} x_k \\ u_{1_k} \end{Bmatrix} + \begin{bmatrix} 0 \\ G_{12} \end{bmatrix} u_{2_k} \qquad (11)$$

The optimal time-invariant control law for this system can now be computed using the method described in references 13 to 15. The control law can be expressed as

$$u_{2_k} = H_{11} x_k + H_{12} u_{1_k}$$

$$= H_{11} x_k + H_{12} (u_k + W) \qquad (12)$$

Substituting for u_{2_k} as

$$u_{2_k} = \frac{u_{k+1} - u_k}{\Delta T}, \quad \Delta T = \text{time interval}$$

$$u_{k+1} = H_{11}x_k \, \Delta T + (H_{12} \, \Delta T + 1)u_k + H_{12}W \, \Delta T, \quad u_{k=0} = u_0 \qquad (13)$$

The initial condition u_0 can be obtained from the expression for the minimum performance index (ref. 16) as

$$u_0 = (P_{22}^{-1} \, P_{12}^{T} \, x_0 + W)$$

where $\qquad\qquad\qquad\qquad\qquad\qquad\qquad\qquad\qquad\qquad\qquad\qquad$ (14)

$$P = \begin{bmatrix} P_{11} & P_{12} \\ P_{12}^{T} & P_{22} \end{bmatrix}$$

is the steady-state solution of the Riccati equation. This matrix is already obtained during computation of the constant, state feedback gain matrix above.

Substituting the above control law, the original system equations can now be solved by simulation on a digital computer as usual.

IMPLEMENTATION OF THE CONTROL LAW

Introduction

In this section, two methods of implementing the digital, state feed-back, optimal control law derived in the previous section are discussed briefly. Their relative advantages and disadvantages are discussed under "Conclusions."

Forced-Regulator Method

The dichotomy of this method of implementation can be described as follows. By running a few trial simulations, the values of the rates of

throttle and elevator are found which will flare the airplane from the nominal glide slope (-3° in the present case) to an acceptable touchdown condition in the absence of any winds, either gusts or shears. The values of these ramps on the throttle and elevator are now stored and forced on the airplane (in an open-loop manner) even when it is flaring through a given wind shear field. However, the perturbations in the state variables from the baseline no-winds trajectory due to the effect of the wind shears are now used to close the loop and generate an additional control using the control law derived in the previous section. The total control therefore consists of two parts: (1) the open-loop ramps (i.e. values of the rates of throttle and elevator) derived for the no-wind flare performance and (2) the state feedback, optimal control law designed to drive the deviations from the baseline no-wind trajectory to zero. The two parts are added algebraically to yield the total control required. The particular structure of the controller leads to the name "Forced-Regulator Method."

Regulator Method

The concept of this method is very simple. The differences between the terminal (touchdown) conditions and the initial glide slope are supplied as the initial conditions for the optimal, state feedback control law derived in the previous section. The terminal conditions used could be either those on an equilibrium trajectory with sink rate of 0.61 m/s (2 ft/s) or any desired touchdown conditions. The latter case was extensively studied in previous works of the author (refs. 8-10, 12).

A few runs were simulated using the terminal conditions on an equilibrium trajectory with a sink rate of 0.61 m/s (2 ft/s) to derive the initial conditions for generating the closed-loop control law, but the results were found to be very unsatisfactory, and so are not presented here. The disadvantages are discussed in detail under "Conclusions."

RESULTS

In this section the performance of the discrete, optimal control law implemented using the Forced-Regulator Method described in the previous

section is evaluated. The plant dynamics used are those of the TCV Boeing-737 research aircraft at NASA/LaRC. The aircraft is assumed to be on a 3° glide slope when the flare maneuver is initiated at a specified height. Simultaneously, the aircraft enters one of the example shear profiles tabulated in table 1.

Note that, even though an optimal feedback gain matrix was computed for each case, for purposes of simplicity in onboard implementation of the control law, it was decided to compute only one gain setting for the shear profile A, and to use the same setting for all the cases simulated. This procedure would eliminate the need for changing the gain setting onboard the aircraft, each time a different shear profile is encountered by the aircraft. The time response curves presented indicate the performance of the Forced-Regulator Method of implementation of the control law described earlier.

After a few initial trial simulations, it was found that, in the absence of any winds, ramping back the elevator at the rate of 0.7835 deg/s and the throttle at the rate of 4.193 deg/s yielded a very satisfactory flare performance (fig. 2). Touchdown occurred at 6.2 s at a horizontal distance of 393.8 m (1,292 ft). The sink rate at touchdown was 0.67 m/s (2.186 ft/s) and the pitch attitude was 2.662°. The value of the thrust was reduced to 10,822 N (2,433 lb). It was noted, however, that the value of the sink rate at touchdown was very sensitive to the command rate of the elevator.

With the flare trajectory thus obtained by forcing the ramps on the elevator and the throttle as a nominal or baseline trajectory, a wind shear field of profile A (table 1) was forced on the airplane. The state feedback optimal control law was activated to generate an additional control to null the deviations of the aircraft from the nominal trajectory (fig. 2). Figures 3a to 3c show the flare performance as the aircraft flew through the shear profile A. The touchdown occurred at 6.1 s at a horizontal distance of 387.7 m (1,272 ft) from the initiation of the flare maneuver, at a pitch attitude of 4.387°. The sink rate at the touchdown was 0.66 m/s (2.163 ft/s) and the flare was initiated at 15.54 m (51 ft) above ground level.

13

Table 1.   Inertial Wind Profiles Simulated.

Profile	Wind Parameters
A	Tailwind increasing at 10 kn/30.48 m (100 ft) Downdraft increasing at 2 kn/30.48 m (100 ft)
B	Headwind increasing at 10 kn/30.48 m (100 ft) Updraft increasing at 2 kn/30.48 m (100 ft)
C	Headwind increasing at 10 kn/30.48 m (100 ft) Downdraft increasing at 2 kn/30.48 m (100 ft)
D	Headwind increasing at 5 kn/30.48 m (100 ft) Updraft increasing at 2 kn/30.48 m (100 ft)
E	Tailwind increasing at 5 kn/30.48 m (100 ft) Downdraft increasing at 2 kn/30.48 m (100 ft)
F	Tailwind increasing at 15 kn/30.48 m (100 ft) Downdraft increasing at 2 kn/30.48 m (100 ft)
G	Headwind increasing at 15 kn/30.48 m (100 ft) Updraft increasing at 2 kn/30.48 m (100 ft)
H	Headind increasing at 15 kn/30.48 m (100 ft) Updraft increasing at 5 kn/30.48 m (100 ft)

Figure 3b shows that the engines were throttled down to reduce the thrust at touchdown to 10,924 N (2,456 lb). The elevator assumed a negative value to provide the necessary pitch-up attitude.

Figure 3c shows the velocity components of the wind at the wing and those felt by the wing.

Figures 4a to 4c demonstrate the flare maneuver performed by the aircraft entering into a wind profile B. It is again noted that, when generating the closed-loop control law for the shear profiles B through H, the optimal gain matrix computed for the shear profile A is used in all the cases, even though, in each case, the optimal gain matrix was computed and found to be significantly different for each case.

It is clear that the reverse of the shear in both the horizontal and the vertical wind velocity components had a significant effect on the elevator history. The touchdown occurred at 6.0 s at a distance of 381.3 m (1,251 ft) from the initiation of the flare. The pitch attitude at touchdown was 1.404°, the sink rate was 0.607 m/s (1.992 ft/s), and the thrust was 10,644 N (2,393 lb). It is found that the flare would have to be initiated at 14.66 m (48.1 ft).

Figures 5a to 5c indicate the flare performance when the aircraft entered the wind profile C. The touchdown occurred at 6.1 s at a distance of 386.8 m (1,269 ft). At touchdown the aircraft had a pitch attitude of 2.513°, a sink rate of 0.658 m/s (2.162 ft/s) and a thrust value of 12,557 N (2,823 lb). The flare was initiated from an altitude of 15.21 m (49.9 ft).

Figures 6a to 6c indicate the flare performance when the aircraft encountered the shear profile D. The touchdown occurred at 6.0 s at a distance of 381.6 m (1,252 ft). The aircraft landed with a pitch attitude of 1.727°, a sink rate of 0.658 m/s (2.162 ft/s), and a thrust value of 10,244 N (2,303 lb). The flare was initiated at an altitude of 14.78 m (48.5 ft).

Figures 7a to 7c illustrate the performance of the aircraft when it flared through the wind profile E. The touchdown occurred at 6.3 s at a distance of 399.9 m (1,312 ft). At touchdown the aircraft had a pitch attitude of 3.841°, a sink rate of 0.668 m/s (2.194 ft/s), and a thrust value of 10,951 N (2,462 lb). The flare was initiated at an altitude of 15.69 m (51.5 ft).

15

Figures 8 to 10 illustrate the flare performance of the aircraft when it encountered a fairly severe shear of ±15 kn/30.48 m (100 ft) in the horizontal wind velocity. Presently, this is very near the maximum value of shear in the horizontal wind component in which the aircraft are allowed to attempt landing.

Figures 8a to 8c show the flare performance of the aircraft when it encountered the shear profile F. The touchdown occurred at 5.9 s at a distance of 375.5 m (1,232 ft). At touchdown the aircraft had a pitch attitude of 4.889°, a sink rate of 0.647 m/s (2.125 ft/s), and a thrust value of 10,319 N (2,320 lb). The flare was initiated at a height of 15.38 m (50.45 ft).

Figures 9a to 9c show the performance in the presence of wind profile G. The touchdown occurred at 5.9 s at a distance of 375.2 m (1,231 ft). The aircraft had a pitch attitude of 1.096°, a sink rate of 0.67 m/s (2.201 ft/s), and a thrust value of 11,405 N (2,564 lb) when it touched down. The flare had to be initiated at an altitude of 14.49 m (47.55 ft).

Figures 10a to 10c illustrate the flare performance of the aircraft when it encountered the shear profile H. In this case, the aircraft encountered an increasing headwind of 15 kn/30.48 m (100 ft) and an increasing updraft of 5 kn/30.48 m (100 ft). This was the most severe shear profile simulated in the present work. The touchdown occurred at 5.8 s at a distance of 369.4 m (1,212 ft). At touchdown, the aircraft had a pitch attitude of 0.2986° (which is barely sufficient to avoid a nose-wheel landing), a sink rate of 0.679 m/s (2.227 ft/s), and a thrust value of 9,857 N (2,216 lb). Because of the extra lift available from the headwind-updraft combination, the aircraft needed to be flared from a much lower attitude of 14.1 m (46.25 ft).

Thus, it is seen that even with the use of a single gain setting (computed for the shear profile A), the forced-regulator method of implementing the control law tends to generate a satisfactory flare trajectory in the presence of widely different wind shear conditions.

CONCLUSIONS

From the time response curves presented in the previous section for the different shear profiles considered, it is clear that the forced-

16

regulator method of implementing the control law developed in an earlier section is quite capable of performing the required flare maneuvers in the presence of widely differing shear conditions.

It is noted that, in spite of using a single gain setting (computed for the wind shear profile A) for all the cases, three of the touchdown conditions, viz the time required for touchdown after initiation of the flare, the distance traveled to touchdown, and the thrust value at touchdown, were found to be relatively insensitive to the wind conditions. The time required to touch down varied from 5.8 s to 6.3 s. The horizontal distance required to touch down varied from 369.4 m (1,212 ft) to 399.9 m (1,312 ft) - a dispersion of ±15.2 m (50 ft), which is considered extremely good for the widely differing wind shear conditions studied. The thrust value at touchdown varied from a minimum of 9,857 N (2,216 lb) to a maximum of 12,557 N (2,823 lb).

Two variables, the pitch attitude at touchdown and the altitude at which the flare should be initiated [to obtain a sink rate of approximately 0.64 ± 0.04 m/s (2.1 ± 0.12 ft/s) at touchdown], were found to be sensitive to the wind shear profiles encountered. The value of the pitch attitude at touchdown varied from one barely sufficient to avoid nosewheel landing (0.2896°) to a very robust pitchup (4.889°). It was found that the aircraft landed with a lower pitch attitude than the no-wind condition (fig. 2) for a headwind and a higher attitude for a tailwind. This type of behavior is to be expected because of the relative gain (loss) of lift from the resulting headwind (tailwind) for the same pitch attitude.

The altitude at which the flare should be initiated to achieve a sink rate of approximately 0.64 m/s (2.1 ft/s) at touchdown also showed some variation. The minimum value of this altitude was 14.1 m (46.25 ft) and the maximum value was 15.7 m (51.54 ft). While this dispersion in the altitude may not be too great, it is considerd to be a disadvantage. For practical purposes, it would be of great convenience to the pilot (or the autopilot) to initiate the flare maneuver every time from the same decision altitude, instead of differing decision altitudes for different wind conditions.

During the course of this project, the author has reported extensive studies of many different types of control laws (refs. 1, 2, 8-10, 12). The types of control laws studied varied from time-varying gain to constant

17

gain type, in the absence of any winds to the inclusion of a new wind shear model developed by the author (ref. 10), and from the open-loop type of control law, and the pure regulator type control law to the forced-regulator type of implementation discussed in the present report. The forced-regulator method of implementation of the control law was considered to have the following advantages:

(1) It was easy to come up with a baseline flare trajectory (in the absence of any winds) by imposing two open-loop ramps on the elevator and throttle.

(2) The additional control could be generated by feeding back the difference between states due to the winds encountered and the states due to no wind conditions.

(3) Most of the conditions at touchdown (except the pitch and the decision height from which flare would be initiated) were found to be insensitive to the widely differing wind shears simulated. This was observed in spite of the fact that a single gain-setting was used for all the cases.

The disadvantages of this method of implementation were mainly twofold:

(1) The baseline trajectory in the absence of any winds was found to be extremely sensitive to the rate at which the elevator was commanded. A very small difference in the command rate resulted in either no touchdown (with even a slight rate of climb achieved) within the duration of time for which the simulations were performed or a very hard touchdown, both of which are generally unacceptable.

(2) It is required to select slightly different decision altitudes (to initiate the flare maneuver) for different wind profiles.

The pure regulator type of implementation of the control law was also studied extensively by the author (refs. 8-10) and was found to have a single, but very important disadvantage - an initial increase in the sink rate of the aircraft before it decreased to the desired touchdown value. It was determined that this significant increase in the sink rate was solely due to the way in which the initial conditions were described for that problem. The large error in the glide-slope trajectory and the

18

shallow trajectory (either trimmed or otherwise) at the desired touchdown sink rate introduced highly transient behavior in the perturbed trajectory, and this was responsible for the significant reversal in the sink rate in the initial stage.

From the extensive study of the different types of control laws for performing the flare maneuver in the presence of winds, it is evident that much work is needed in the area of developing insensitive control laws to solve this very difficult problem. Further work is also needed to conduct online estimation of the wind parameters and to reduce the sensitivity of the touchdown parameters to the differing wind conditions. The results of implementing the various types of control laws reported in the present work along with that reported in the references should form a base for further work in solving this very important problem.

REFERENCES

1. Nadkarni, A.A.: Digital Flare Law Development. Final Report, NASA contract NAS1-14193-34, Dec. 1977.

2. Nadkarni, A.A.: Comparative Study of Flare Control Laws. Progress Report, NASA Grant NSG 1480, July 1978.

3. Halyo, N.: Development of an Optimal Automatic Control Law and Filter Algorithm for Steep Glide Slope Capture and Glide Slope Tracking. NASA CR-2720, Aug. 1976.

4. Halyo, N.: Development of a Digital Automatic Control Law for Steep Glide Slope Capture and Flare. NASA CR-2834, June 1977.

5. Etkin, B.: Dynamics of Atmospheric Flight. John Wiley and Sons, Inc. 1972.

6. Roskam, J.: Flight Dynamics of Rigid and Elastic Airplanes. Roskam Aviation and Engineering Corporation (KS), 1972.

7. McRuer, D.; Ashkenas, I.; and Graham, D.: Aircraft Dynamics and Automatic Control. Princeton Univ. Press (Princeton, N.J.), 1973.

8. Nadkarni, A.A.: Comparative Study of Flare Control Laws. Progress Report, NASA Grant NSG 1480, Feb. 1979. Also, NASA CR-158114.

9. Nadkarni, A.A.: Comparative Study of Flare Control Laws. Progress Report, NASA Grant NSG 1480, Feb. 1980.

10. Nadkarni, A.A.: Modeling and Controlling Wind Shear Disturbances. Eleventh Annual Modeling and Simulation Conf. (Pittsburgh), May 1-2, 1980.

11. Ogata, K.: State Space Analysis of Control Systems. Prentice-Hall, Inc., 1967.

12. Nadkarni, A.A.: Automatic Flare Transitions Penetrating Wind Shears, Proc. of Joint Automatic Control Conf. (San Fransisco), Aug. 13-15, 1980.

13. Vaughan, D.R.: A Nonrecursive Algebraic Solution for the Discrete Riccati Equation. IEEE Trans. AC, Oct. 1970, pp. 597-599.

14. Vaughan, D.R.: A Negative Exponential Solution for the Linear Optimal Regulator Problem. Proc. JACC, 1968.

15. Vaughan, D.R.: A Negative Exponential Solution to the Matrix Riccati Equation. IEEE Trans. AC-14, Feb. 1969, pp. 72-75.

16. Anderson, B.D.O.; and Moore, J.B.: Linear Optimal Control. Prentice-Hall, Inc. 1971.

20

Subscripts: e = parallel to inertial or earth-fixed
             frame

          b = body fixed frame

          s = stability frame

All angles are positive counterclockwise.

V_{as} = True Air Speed
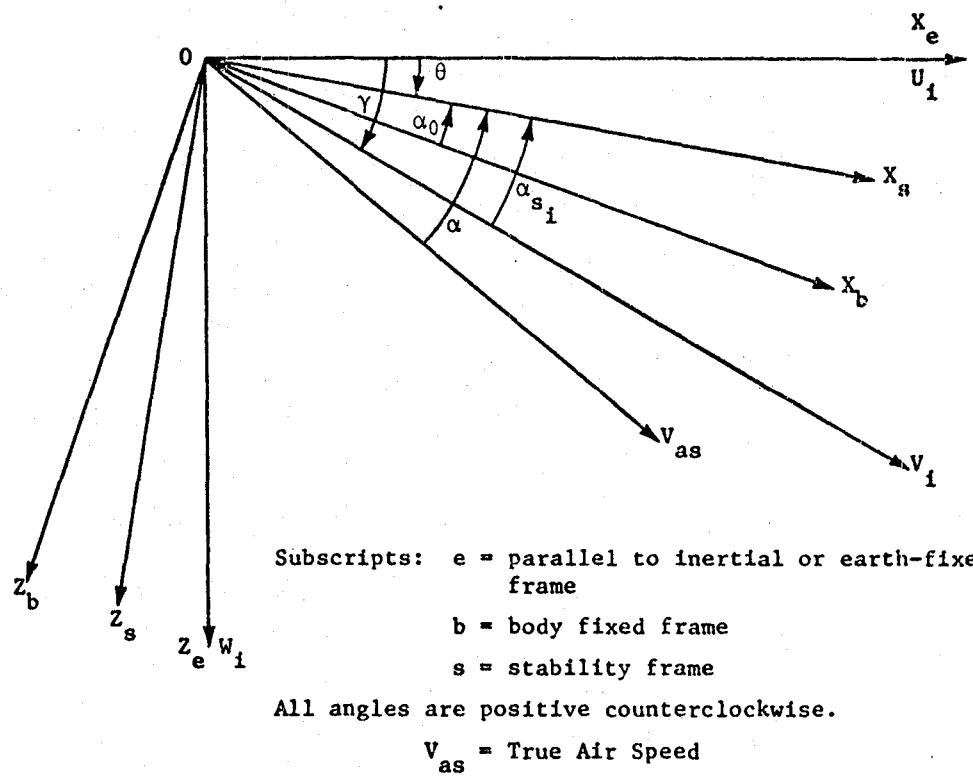
Figure 1. Coordinate frame and flight geometry.

21
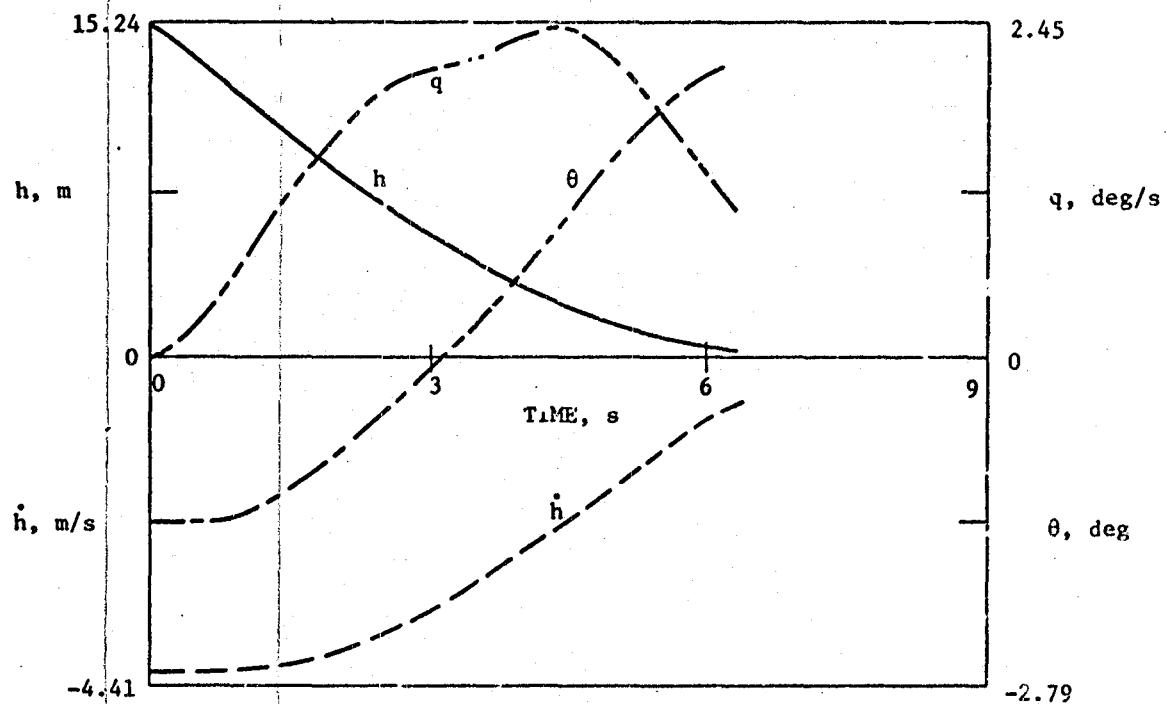
Figure 2a. Flare response: altitude, sink rate, pitch, and pitch rate; no wind.

22
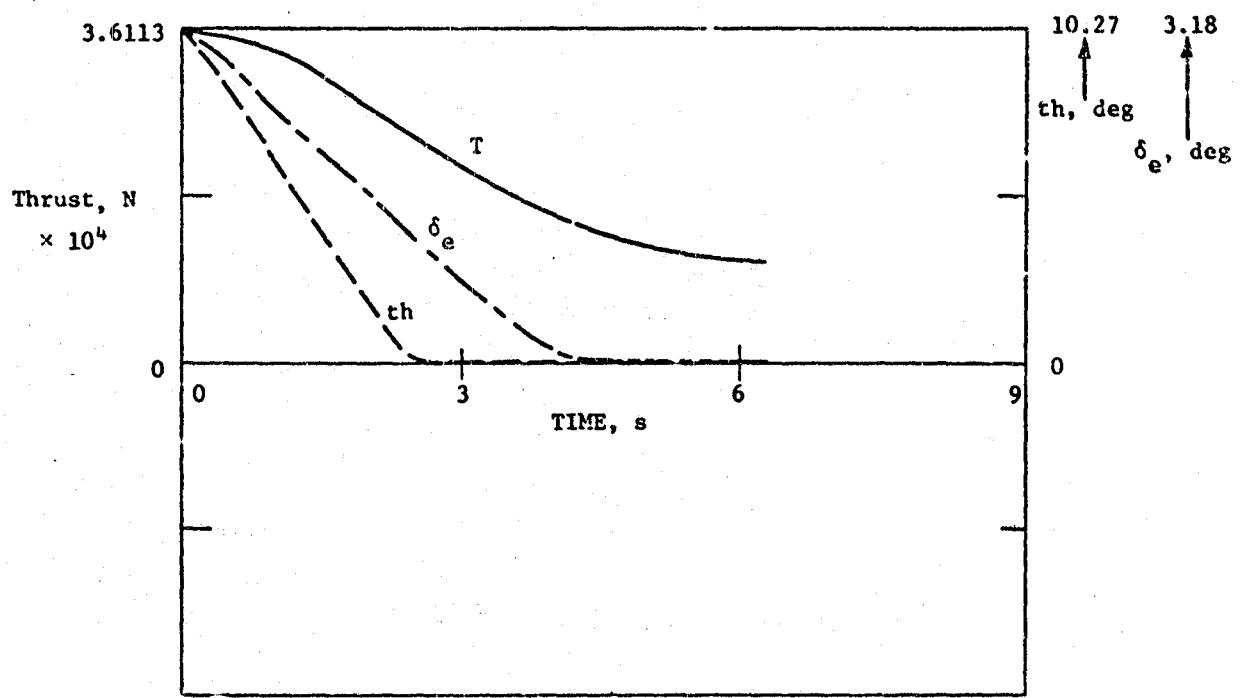
Figure 2b. Flare response: thrust, throttle, and elevator; no wind.
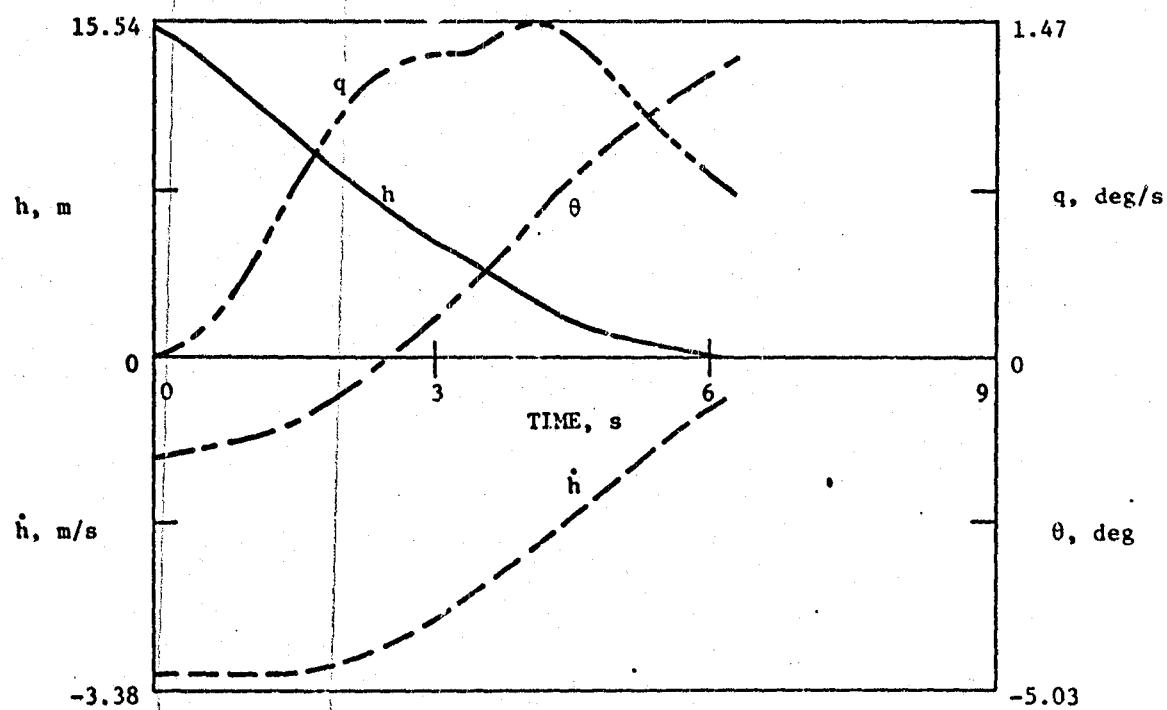
Figure 3a. Flare response: altitude, sink rate, pitch, and pitch rate; wind profile A.
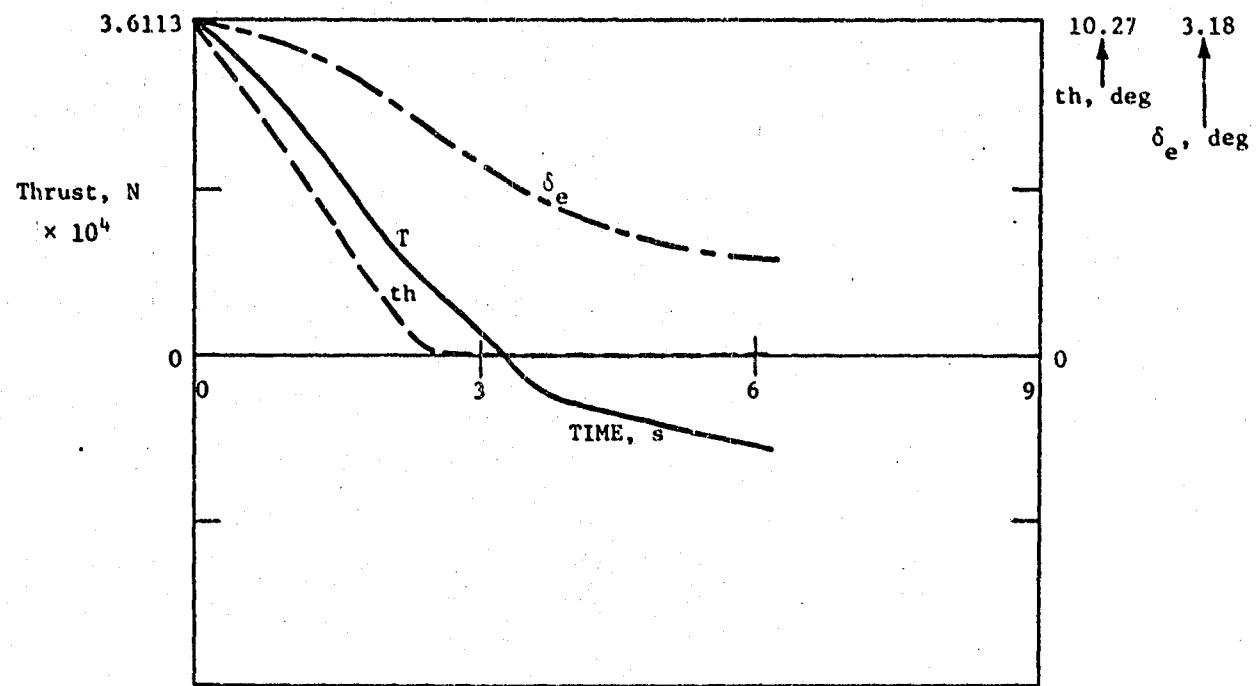
Figure 3b. Flare response: thrust, throttle, and elevator; wind profile A.
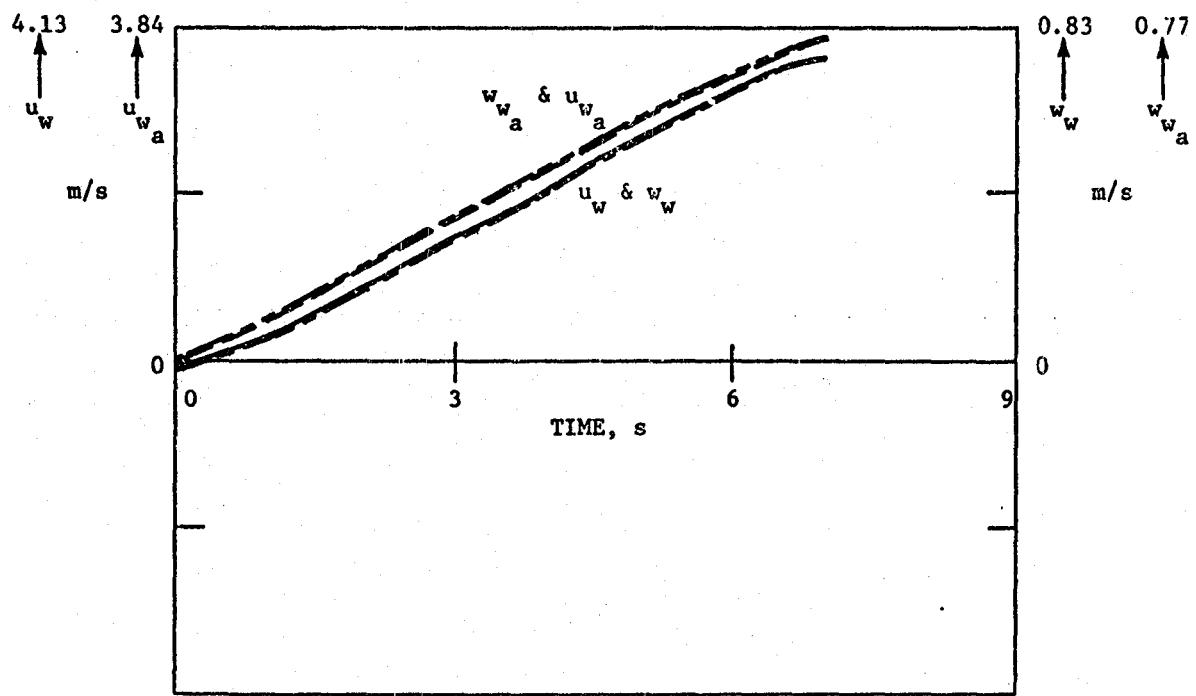
Figure 3c. Flare response: wind velocity components at the wing; wind profile A.
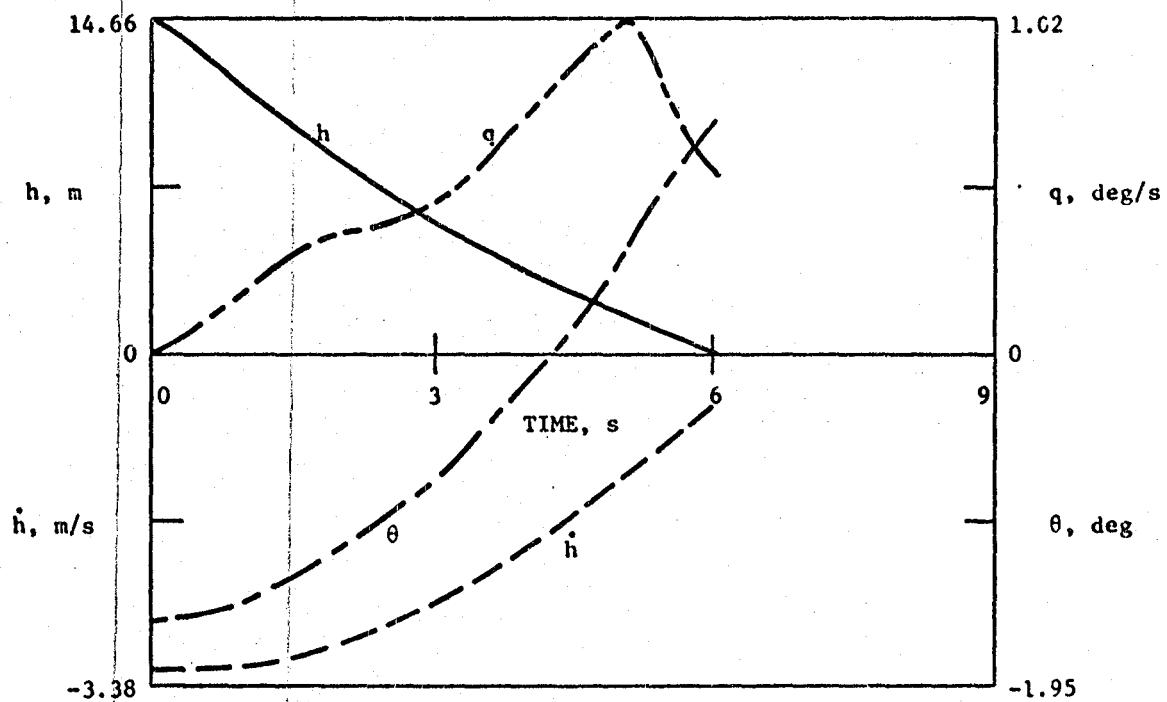
Figure 4a.   Flare response: altitude, sink rate, pitch and pitch rate; wind profile B.

27
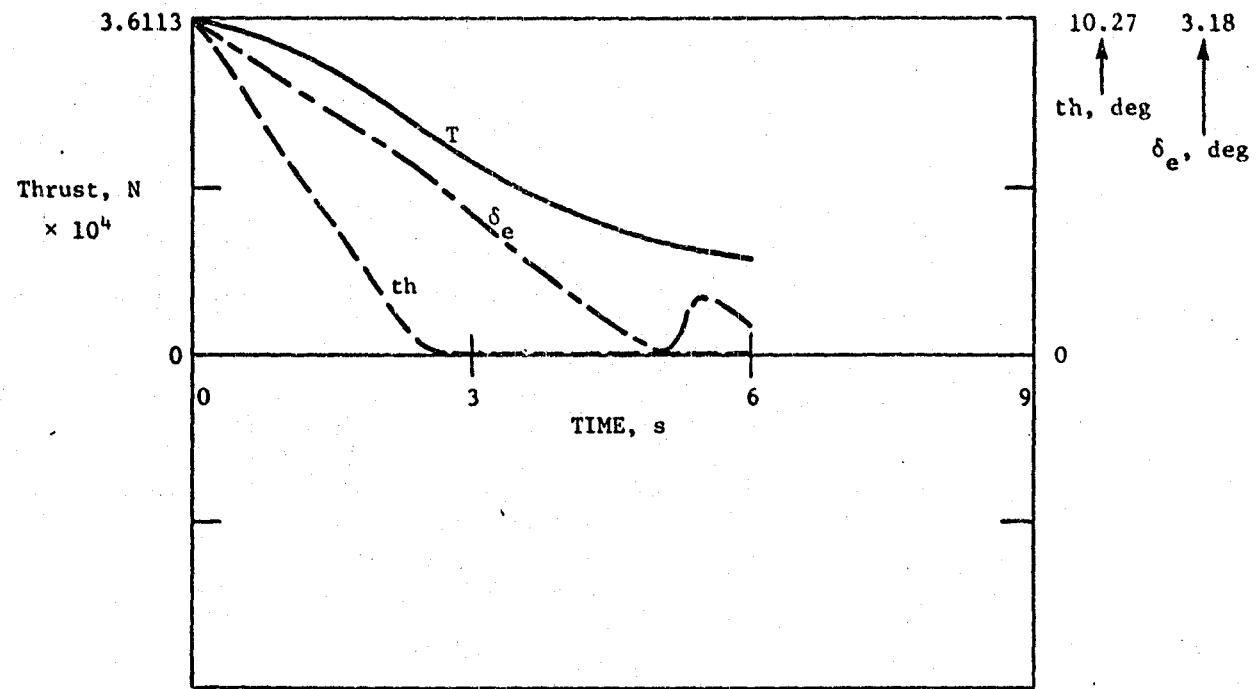
Figure 4b. Flare response: thrust, throttle, and elevator; wind profile b.
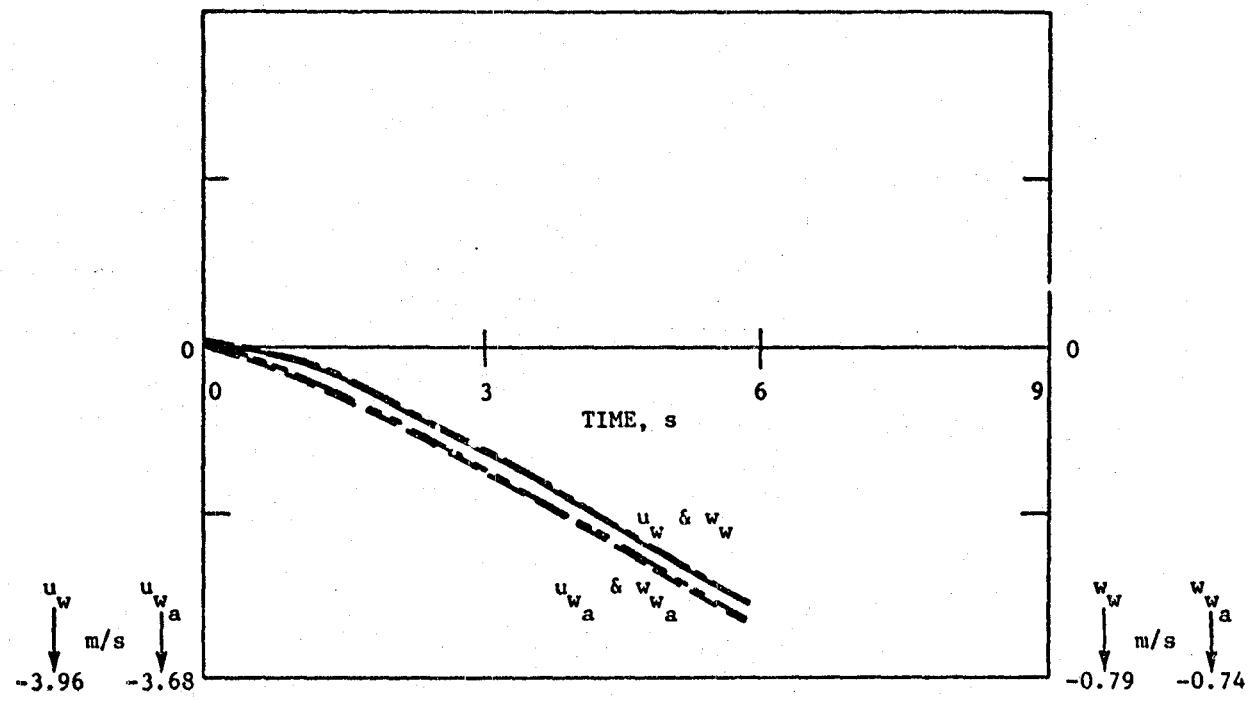
Figure 4c. Flare response: wind velocity components at the wing; wind profile B.

29
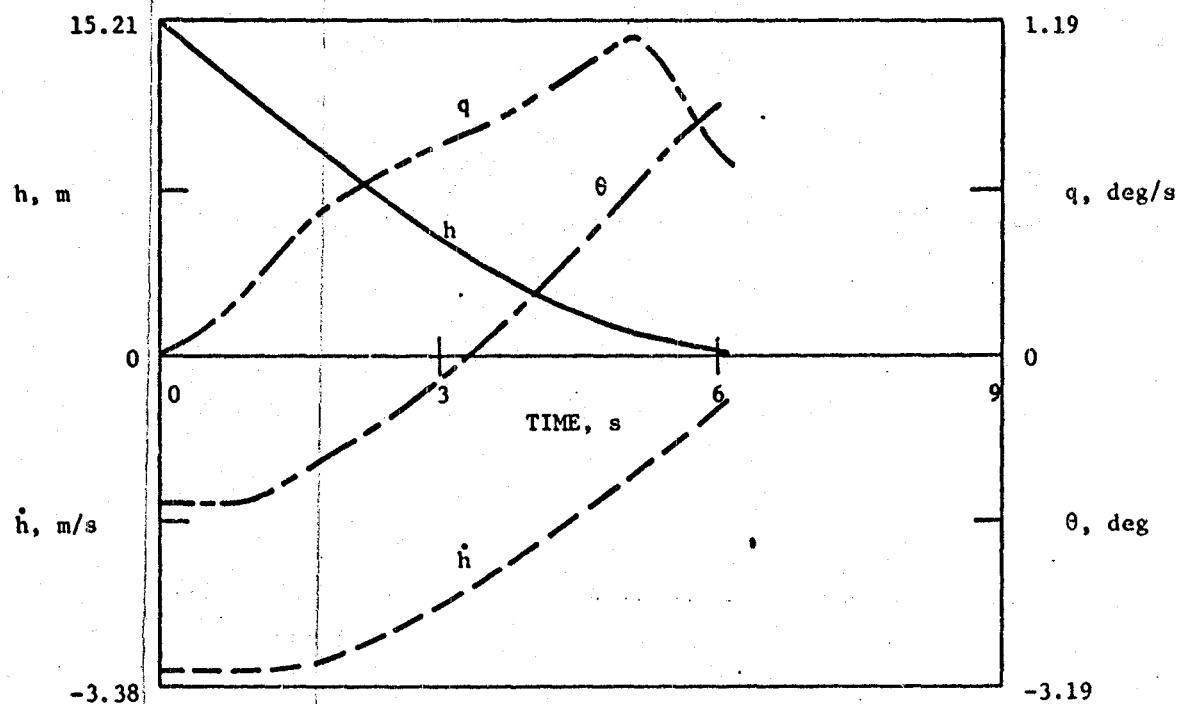
Figure 5a. Flare response: altitude, sink rate, pitch, and pitch rate; wind profile C.
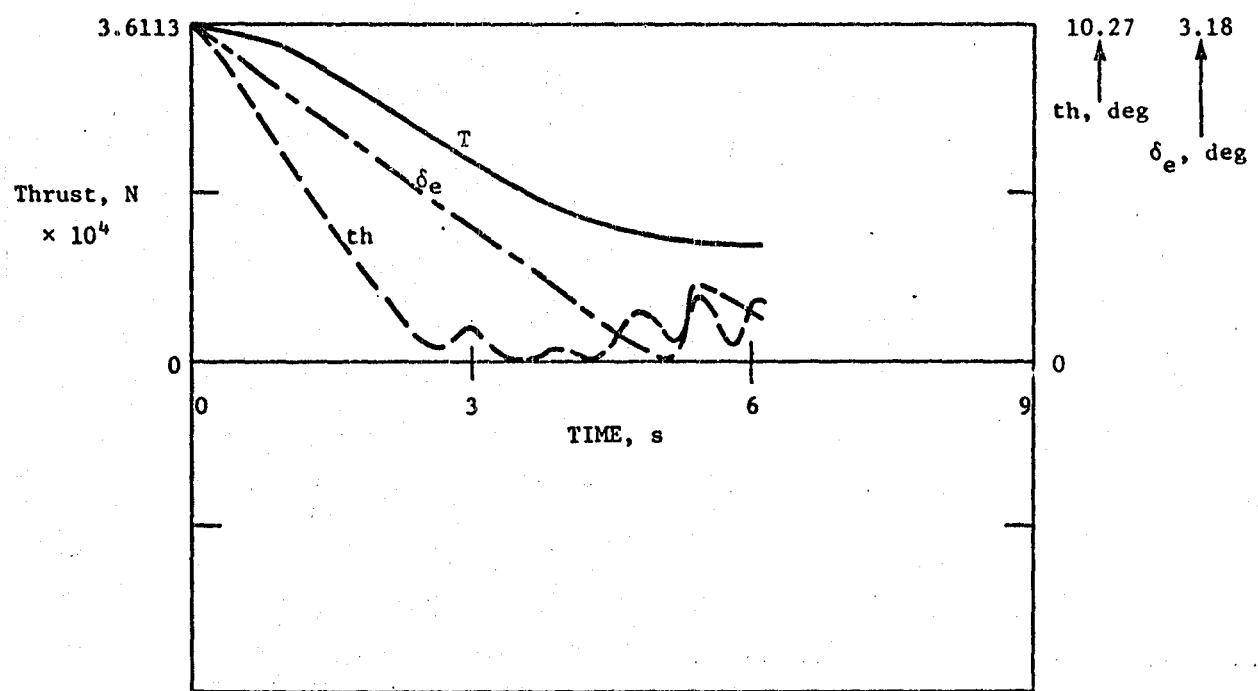
Figure 5b. Flare response: thrust, throttle, and elevator; wind profile C.
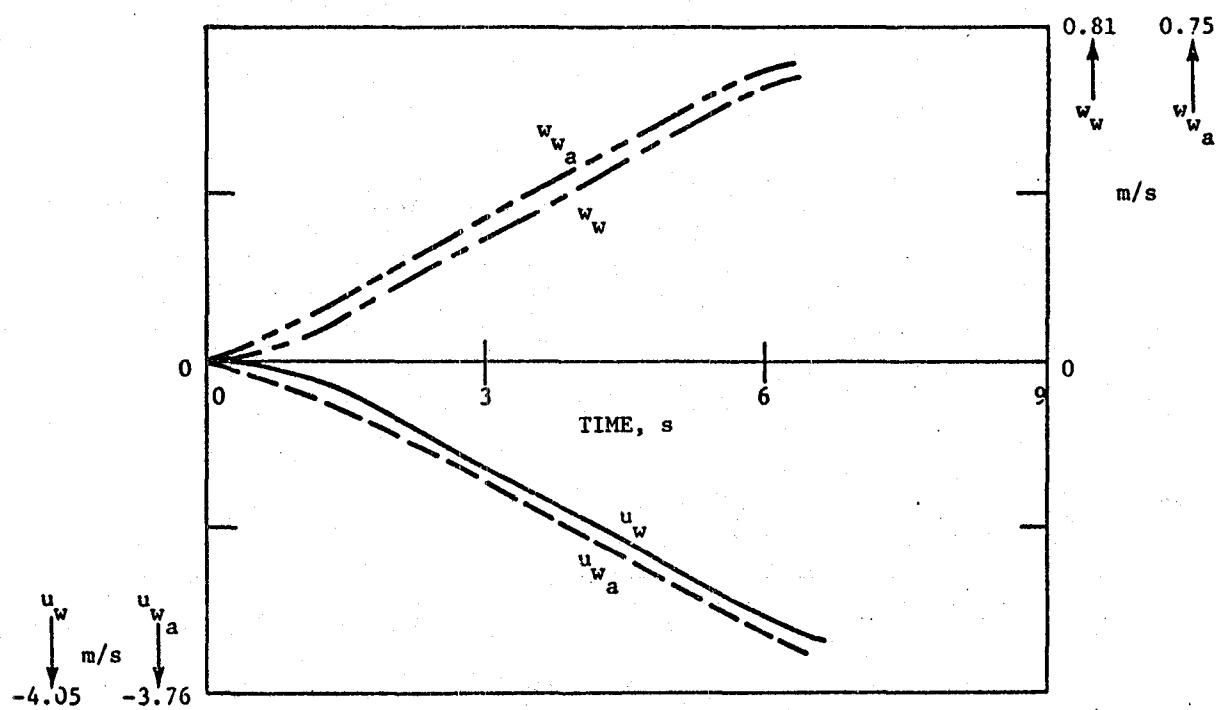
Figure 5c. Flare response: wind velocity components at the wing; wind
profile C.
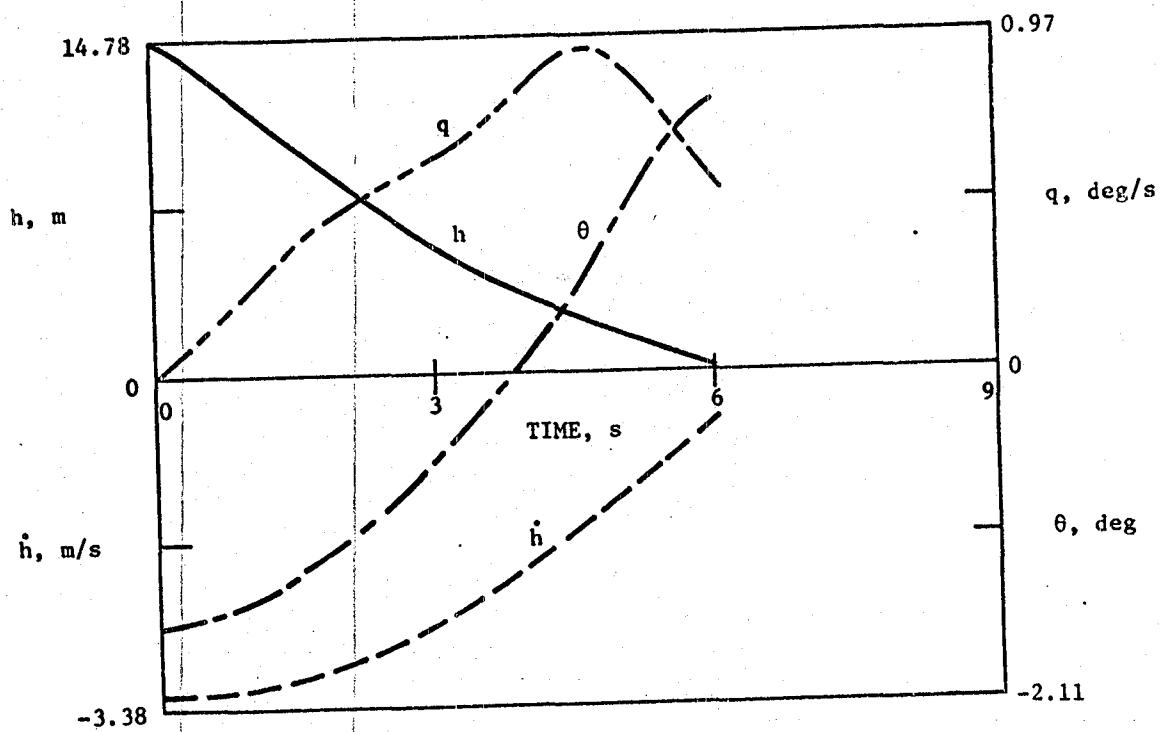
Figure 6a. Flare response: altitude, sink rate, pitch, and pitch rate; wind profile D.

33
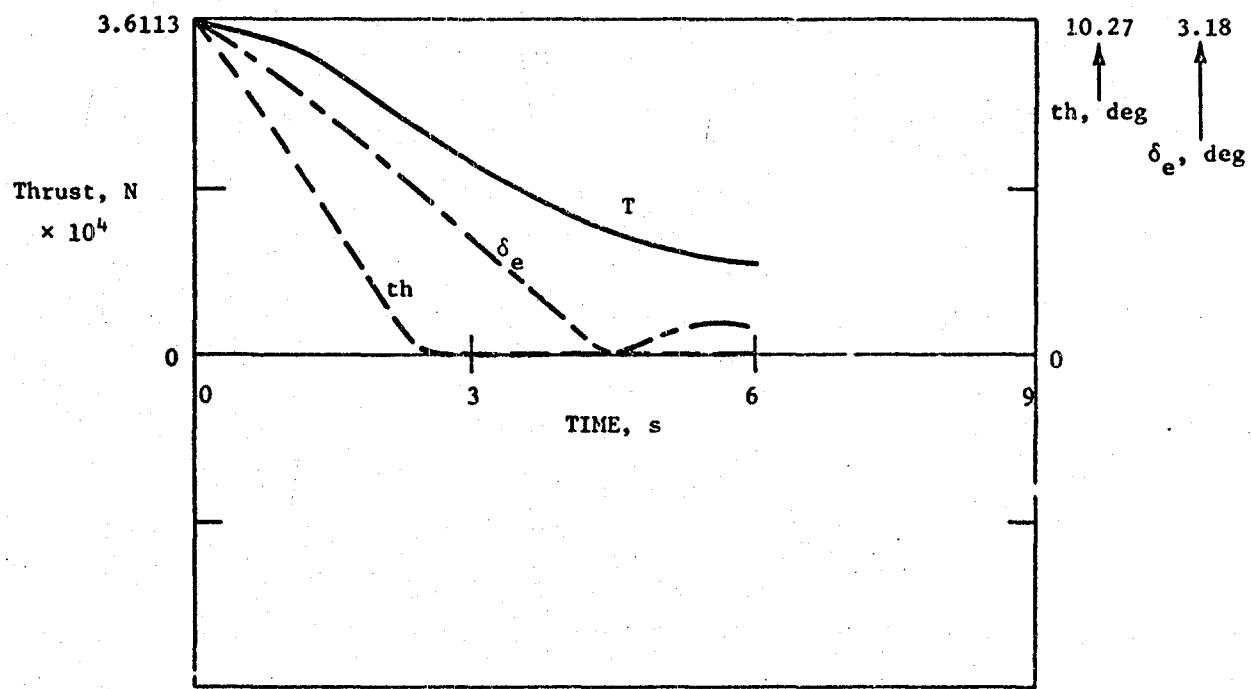
Figure 6b. Flare response: thrust, throttle, and elevator; wind profile D.

34
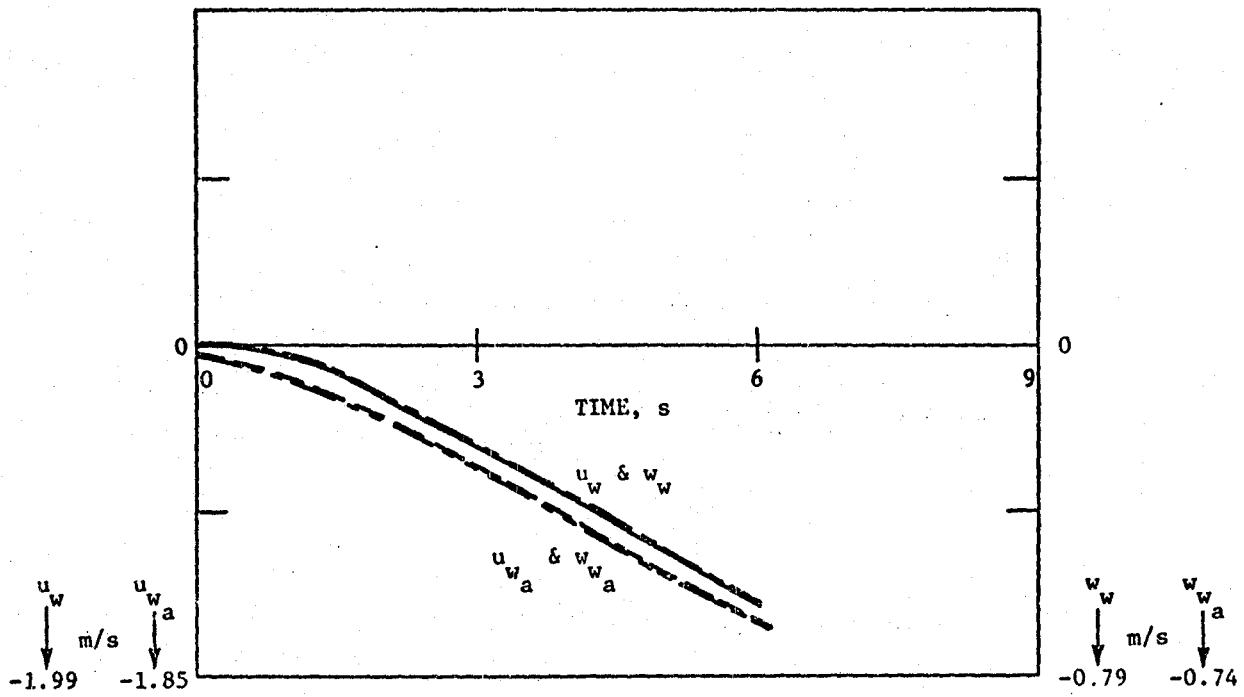
Figure 6c. Flare response: wind velocity components at the wing; wind profile D.
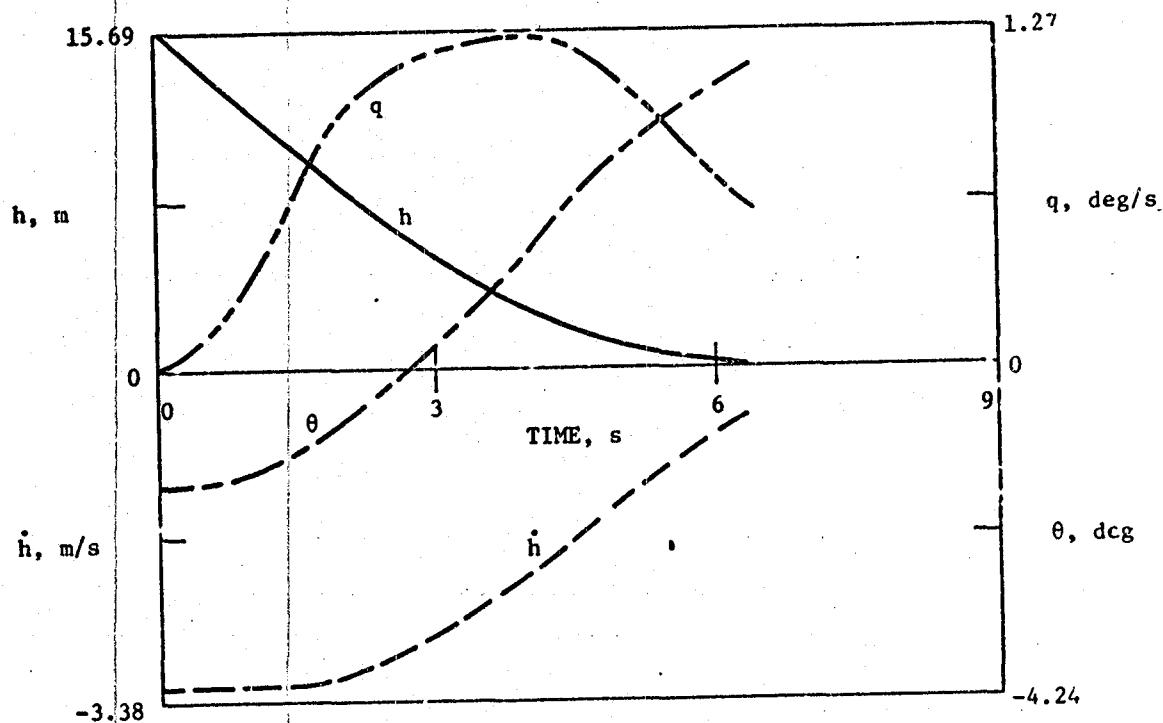
Figure 7a. Flare response: altitude, sink rate, pitch, and pitch rate; wind profile E.
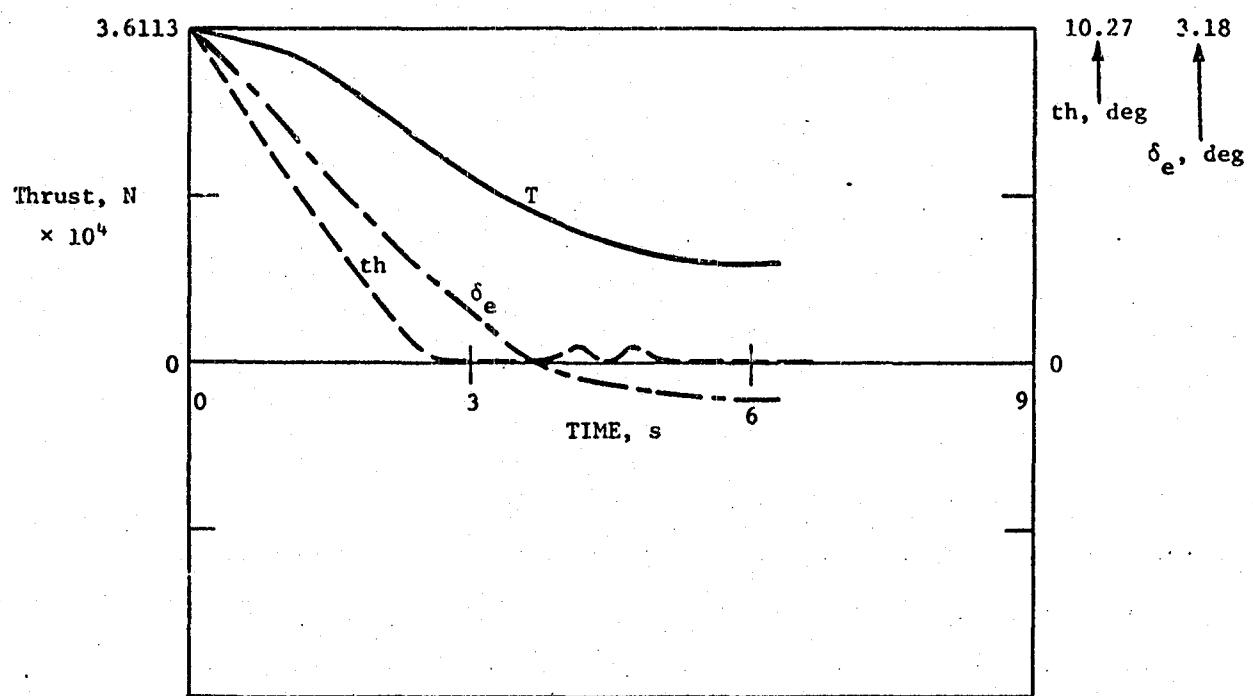
Figure 7b. Flare response: thrust, throttle, and elevator; wind profile E.
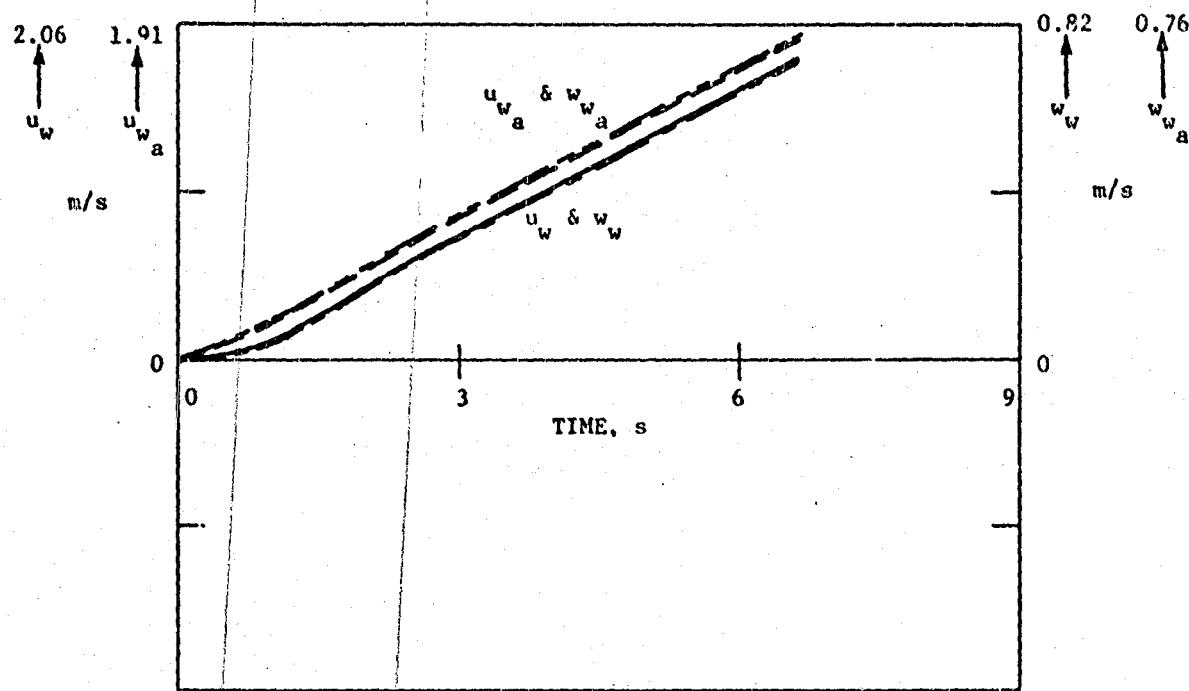
Figure 7c. Flare response: wind velocity components at the wing; wind profile E.
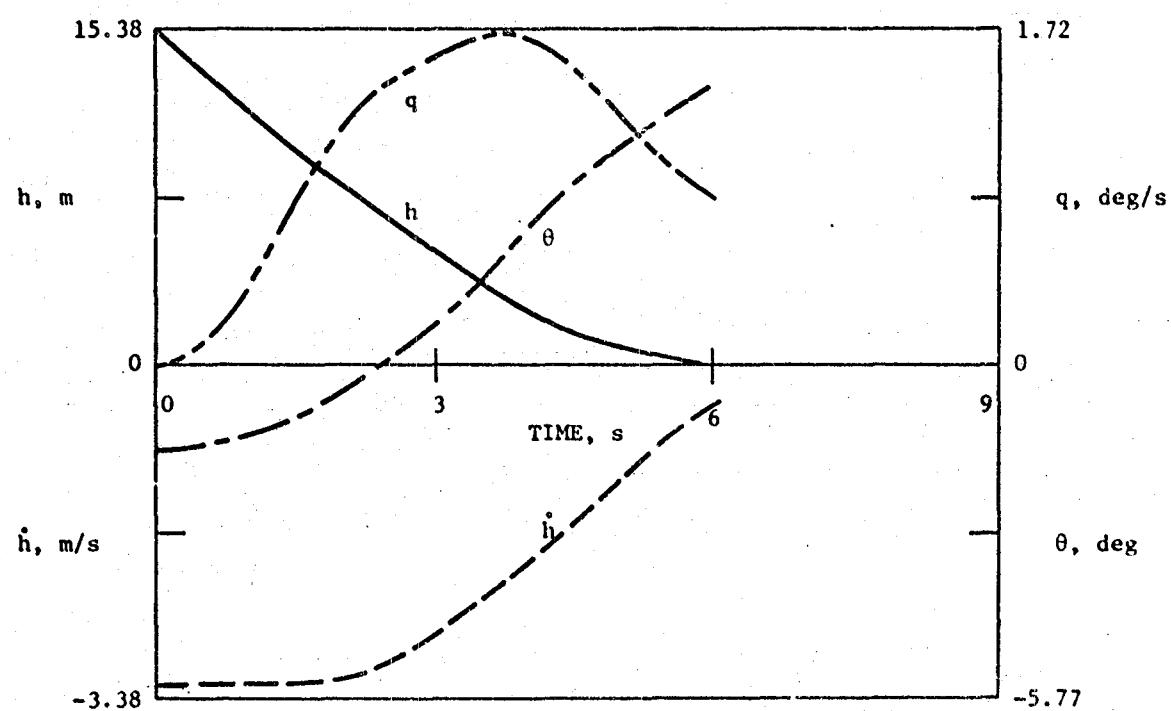
Figure 8a. Flare response: altitude, sink rate, pitch, and pitch rate; wind
profile F.
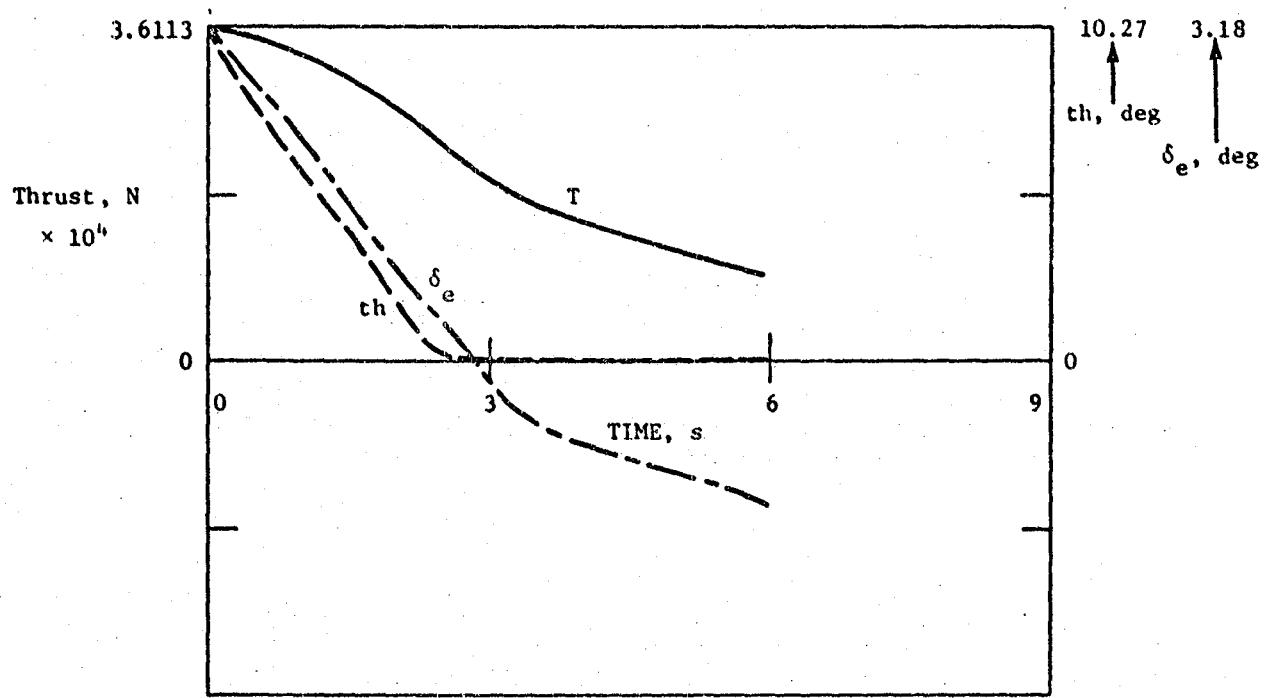
Figure 8b. Flare response: thrust, throttle, and elevator; wind profile F.
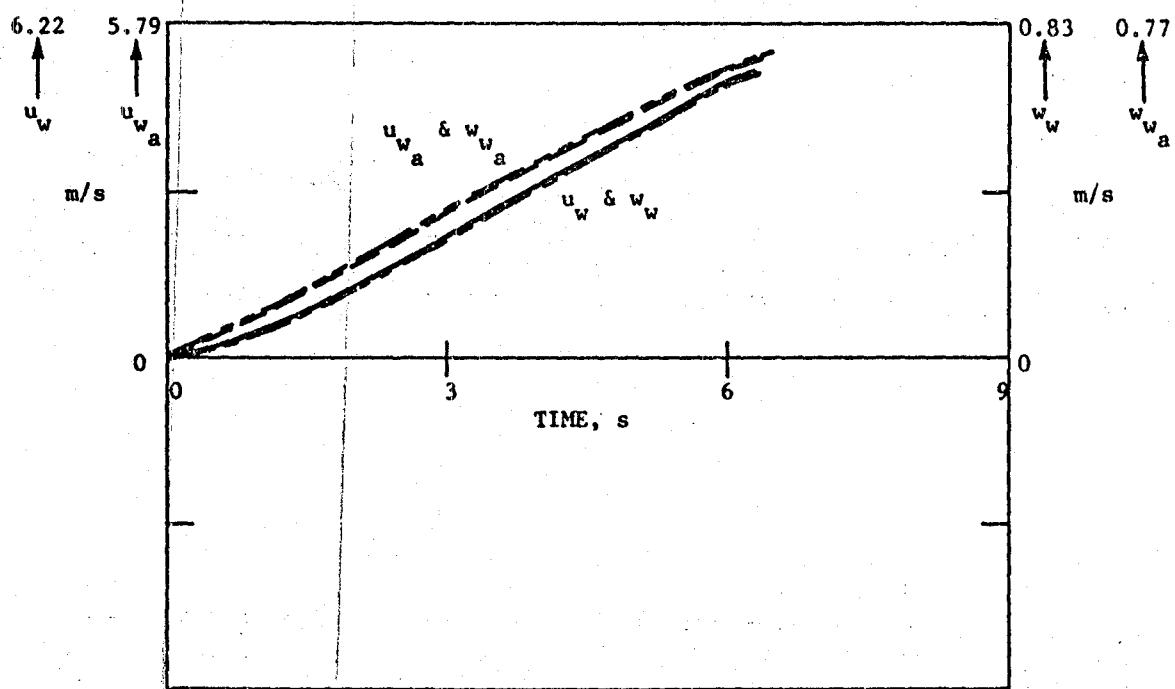
Figure 8c. Flare response: wind velocity components at the wing; wind profile F.
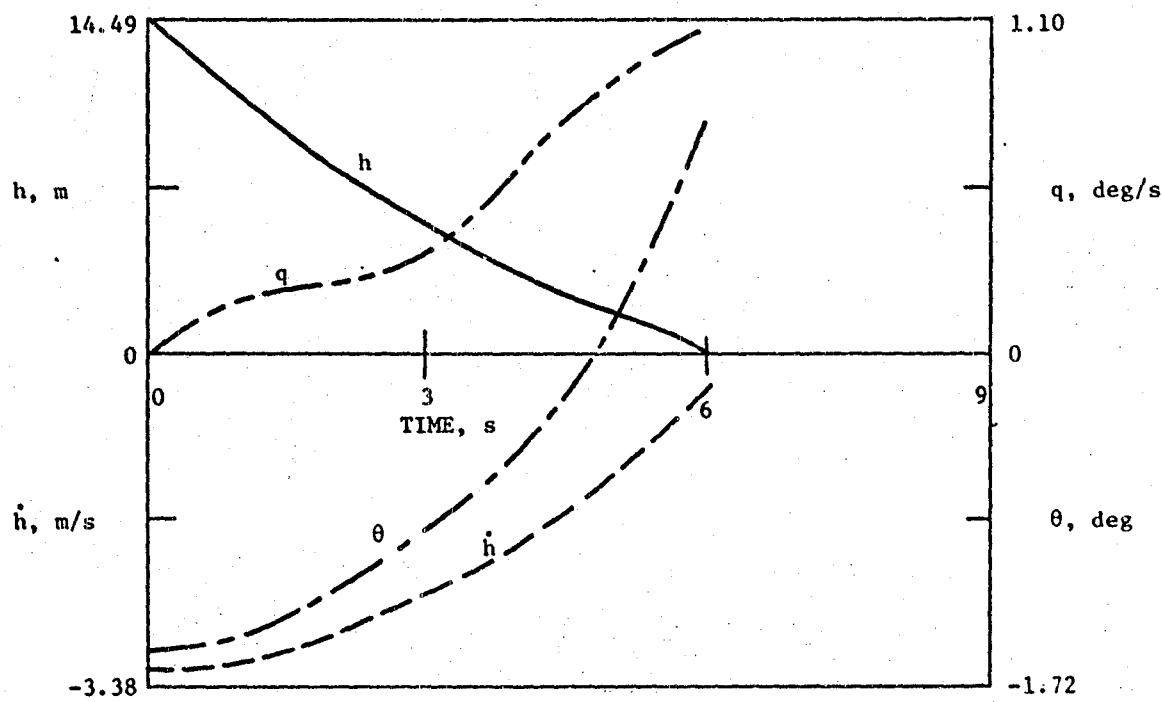
Figure 9a. Flare response: altitude, sink rate, pitch, and pitch rate; wind profile G.
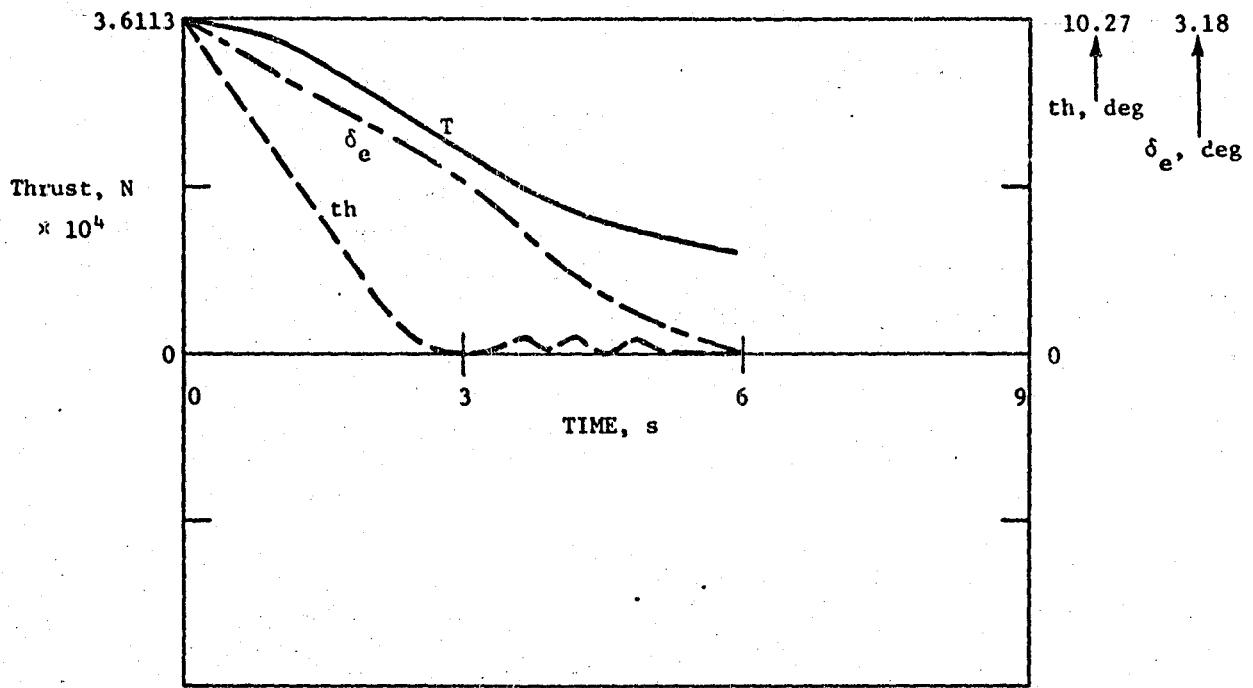
Figure 9b. Flare response: thrust, throttle, and elevator; wind profile G.

43

Figure 9c. Flare response: wind velocity components at the wing; wind profile G.

44
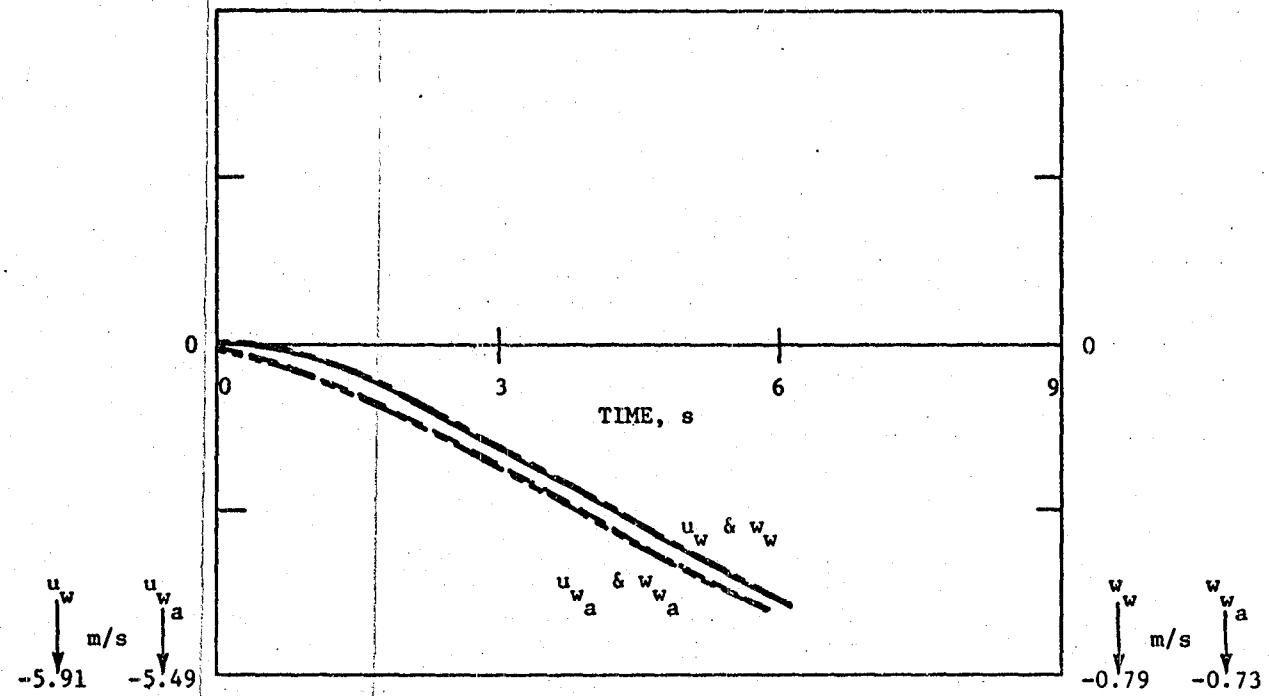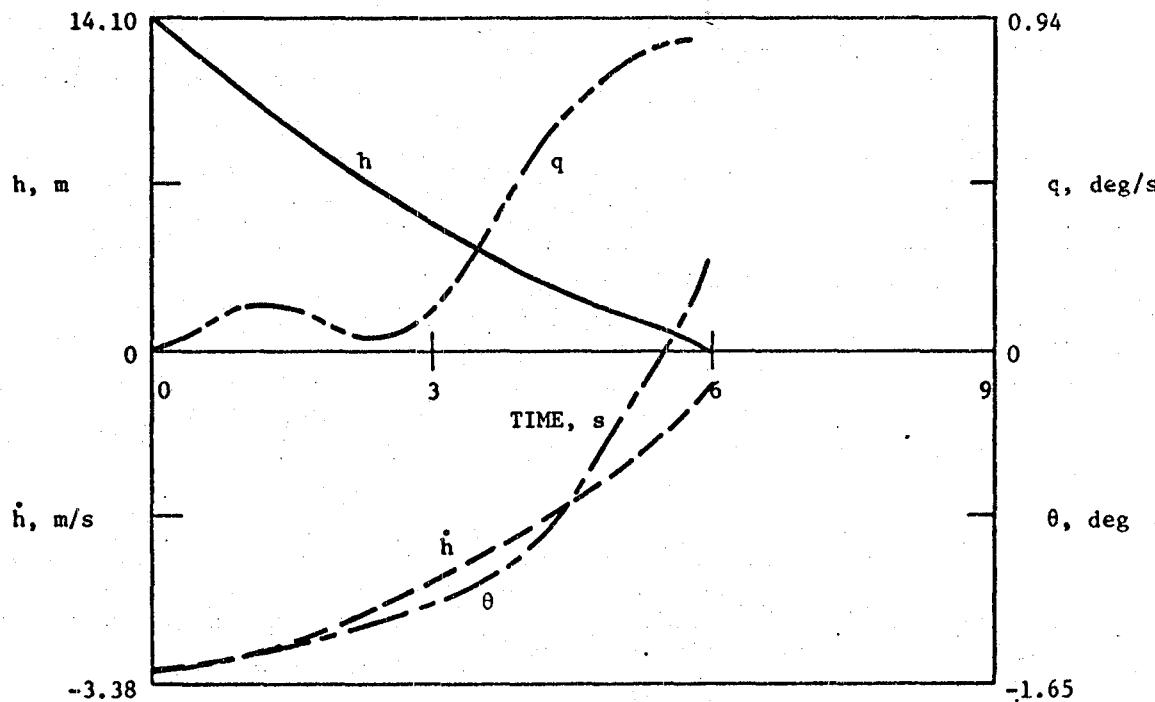
Figure 10a. Flare response: altitude, sink rate, pitch, and pitch rate; wind
profile H.
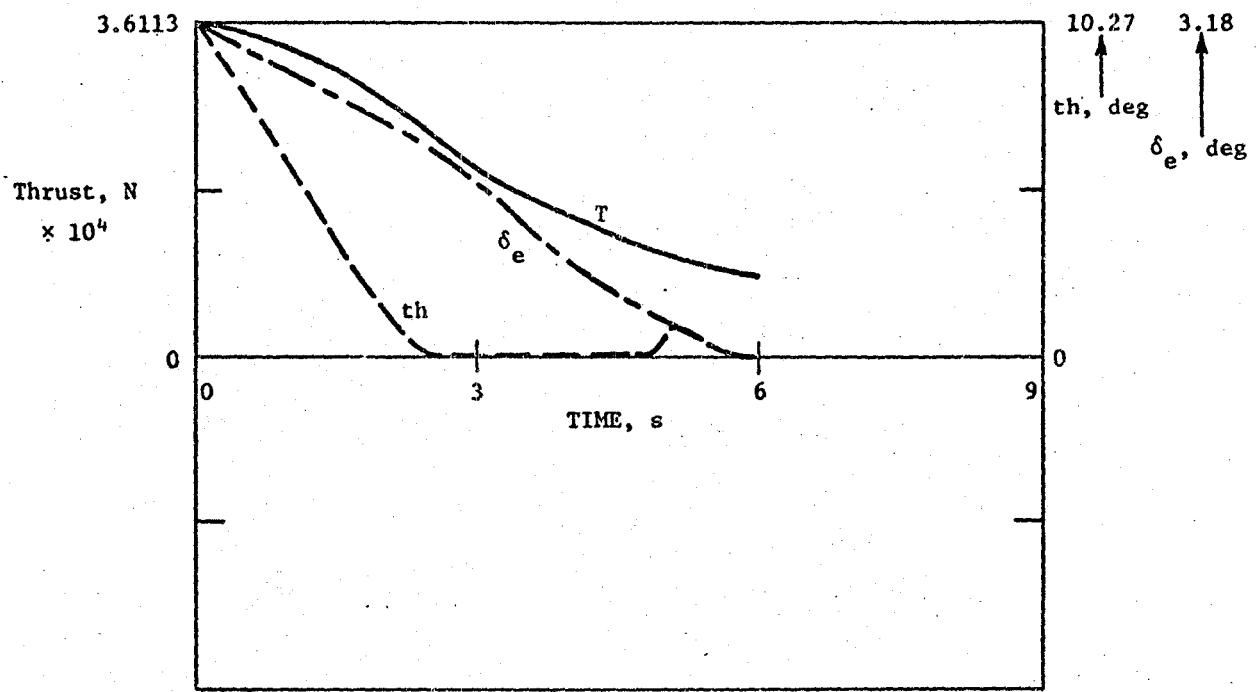
Figure 10b. Flare response: thrust, throttle, and elevator; wind profile H.
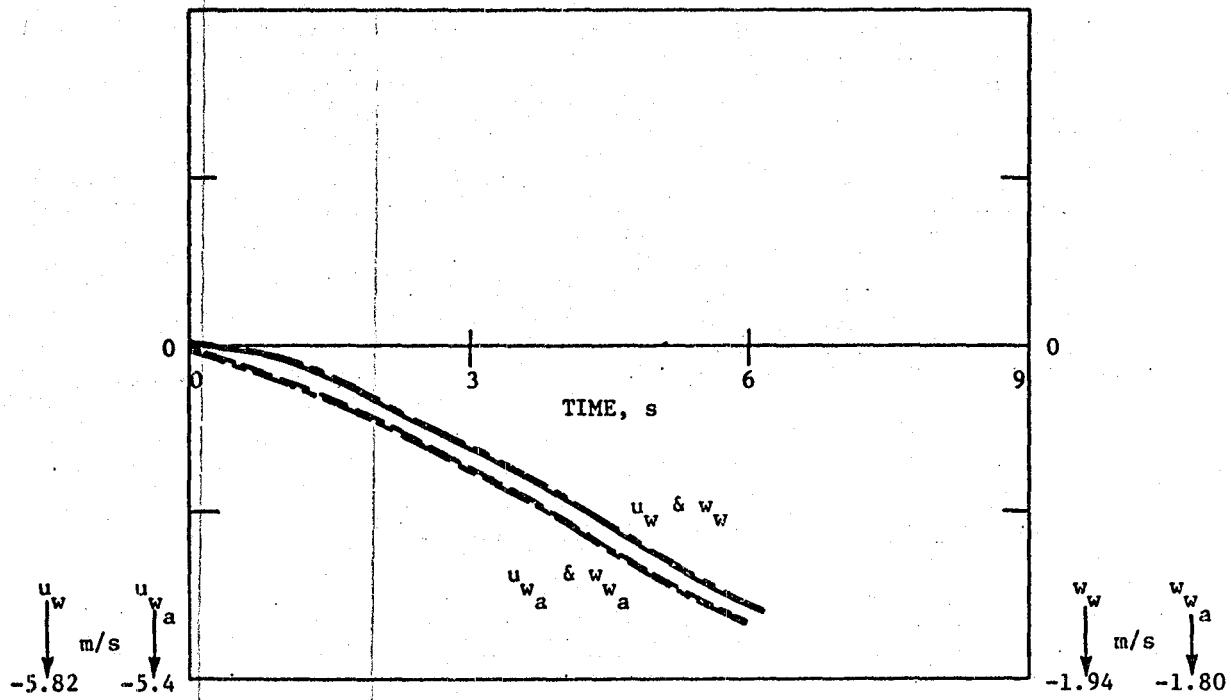
Figure 10c. Flare response: wind velocity components at the wing; wind profile H.

End of Document